Available online at www.sciencedirect.com
ScienceDirect
International Journal of Solids and Structures 44 (2007) 480–506
INTERNATIONAL JOURNAL OF SOLIDS and STRUCTURES
www.elsevier.com/locate/ijsolstr

Limit theorems for gradient-dependent elastoplastic geomaterials

Jidong Zhao *, Daichao Sheng, Scott W. Sloan, Kristian Krabbenhoft

Department of Civil, Surveying and Environmental Engineering, Geotechnical Research Group, School of Engineering, The University of Newcastle, Callaghan, NSW 2308, Australia

Received 13 February 2006; received in revised form 20 April 2006
Available online 7 May 2006

Abstract

In this paper, the limit theorems proposed by Drucker and co-workers are reformulated to address a class of gradient-dependent elastoplastic geomaterials. The gradient effects are accounted for by incorporating strain gradients and their conjugate higher-order stresses into the constitutive descriptions. Gradient-dependent equilibrium equations and higher-order boundary conditions are defined for both statically admissible and kinematically admissible states, and the associated lower bound and upper bound theories are recast for the gradient-enhanced limit theorems. A generalised Drucker–Prager yield criterion, that includes the gradient influence on the deviatoric stress, is proposed and then employed to investigate the collapse loads for soil layers under conditions of generalised plane-strain, simple shear and uniaxial compression. The corresponding lower and upper bounds are found for these problems. It is demonstrated that the predicted collapse bounds are generally dependent on both the conventional and gradient properties, with normalised length scale(s) being present in the results. This feature enables us to give physically reasonable interpretations for size effects and shear banding during material collapse. Comparisons are also made between the gradient-dependent bounds and those obtained through conventional plasticity theories. Influences of model parameters and sample dimensions on the predictions are also discussed. It is shown that the proposed gradient-dependent limit theorems can be used to provide physically meaningful predictions for general geotechnical applications.
© 2006 Elsevier Ltd. All rights reserved.

Keywords: Limit theorems; Strain gradient plasticity; Upper bound and lower bound; Internal length scale; Size effects

1. Introduction

Since the pioneering work of Drucker et al. (1952) and Drucker and Prager (1952), limit analysis has become a powerful tool for predicting the collapse load of practical problems. Conventional limit theorems, including the upper bound and lower bound theorems, are founded on the key assumption of normality between the yield surface and the plastic strain rate vector. Accordingly, restricted forms of the limit theorems can be developed for rigid perfectly-plastic and elastic perfectly-plastic materials. Conventional limit theorems

* Corresponding author. Tel.: +61 2 49215741; fax: +61 2 49216991.
E-mail address: Jidong.zhao@newcastle.edu.au (J. Zhao).

0020-7683/$ - see front matter © 2006 Elsevier Ltd. All rights reserved.
doi:10.1016/j.ijsolstr.2006.04.039

make use of classical plasticity theories in which only the first order stresses and strains are considered in the constitutive descriptions. For various applications involving collapse, however, higher-order gradient terms have proved to be important and ought to be included in the constitutive relations. Theories of strain gradient plasticity have thus been developed during the past two decades, and were originally used to interpret the test results for metallic materials on the microscale. In these theories, higher-order gradient terms are included in the constitutive equations, together with coefficients that represent the length-scale measures of microstructural deformations. The internal length scale of the deformation field is particularly important when interpreting the qualitative and quantitative influence of size effects and strain localisation on collapse behaviour (see, e.g., Chambon et al., 2004 for a recent review of gradient theories).

Compared with metals, geomaterials usually exhibit more complicated mechanical behaviour such as nonlinear elasticity, isotropic hardening, frictional-cohesive strength and dilatancy. In addition to these attributes, they also display gradient-dependent characteristics. For example, experimental observations of localisation phenomena in granular solids have found that the deformed material usually has a strong spatial density variation. Indeed, the formation of shear bands in sands is always characterised by a zone of material with an increased porosity (see, e.g., Vardoulakis and Graf, 1985). In such a region, the strong spatial variation of the material properties suggests that higher gradients of the appropriate physical quantities should be of vital importance. In addition, the existence of micro-structures in geomaterials (i.e., grains, micro-voids, micro-cracks and/or inter-particle contact and friction) may directly or indirectly influence many other features of their behaviour, such as the well-known size effect on material strength. Gradient theories with explicit internal length scales are thus appropriate to link the microstructure of these materials to their macroscopic response. Indeed, a number of gradient-enhanced models have been developed for geomaterials and applied with success. A recent review of the gradient theories developed for geomaterials can be found in Zhao et al. (2005) and Zhao and Sheng (2005).

The features associated with geomaterials provide the motivation to reformulate the conventional limit theorems in the framework of strain gradient plasticity. This motivation is enhanced by the fact that the limit theorems always deal with failure and/or collapse states in the material where gradient effects are mostly pronounced. To the authors' knowledge, the derivation of limit theorems for gradient-dependent elastoplastic geomaterials, and their application to predict collapse, has received little attention in the literature. Even though extremum principles for strain gradient theories have been presented using a number of variational forms (e.g., Smyshlyzev and Fleck, 1996; Fleck and Hutchinson, 1993), these studies focused on the effective properties of polycrystals and are not applicable to geomaterials.

This paper generalises the conventional limit theorems to incorporate strain gradient plasticity, and uses these theorems to predict gradient-dependent lower and upper bound collapse loads for some generalised plane strain problems. The strain gradient theory used builds on the work of Toupin (1962) and Mindlin (1964, 1965). as well as the later contributions of Germain (1973) and Fleck and Hutchinson (1993, 1997). The definition of collapse is assumed to be the same as in conventional plasticity theory; i.e. collapse happens when appreciable changes in the geometry of a structure occur at constant load.

The paper is organised as follows. The strain gradient plasticity used in the study is first introduced. After the stability conditions, normality rule and dissipation behaviour for a gradient-dependent elastoplastic material are recast; the limit collapse state is mathematically described, together with the admissible states and the associated lower and upper bound theorems. Next, the bound theorems so obtained are applied to a class of generalised plane strain problems. A generalised Drucker–Prager yield criterion is also developed to account for the influence of hydrostatic and higher-order stresses on the yielding of geomaterials. Finally, gradient-dependent layers under generalised plane strain, simple shear and uniaxial compression conditions are investigated, and the corresponding lower and upper bounds on the applied loads are found.

2. Strain gradient plasticity and collapse

2.1. Strain gradient plasticity

The strain gradient plasticity theory employed here closely follows the linear elasticity strain gradient theory of Toupin (1962) and Mindlin (1964, 1965), as well as the generalised J_2 plasticity theory suggested by

Fleck and Hutchinson (1993, 1997). The strains and strain gradients are denoted by a second-order symmetric strain tensor $\boldsymbol{\varepsilon}$ and a third-order symmetric strain gradient tensor $\boldsymbol{\eta}$, respectively. In Cartesian coordinates, they are related to the displacement $\mathbf{u}$ as follows:

$$\begin{cases} \varepsilon_{ij} = (u_{i,j} + u_{j,i})/2 \\ \eta_{ijk} = (u_{k,ij} + u_{k,ji})/2 \end{cases} \tag{1}$$

where the strain gradient tensor is symmetric about its first two indices: $\eta_{ijk} = \eta_{jik}$. It is further assumed that the work-conjugates to $\boldsymbol{\varepsilon}$ and η are, respectively, the Cauchy stresses $\boldsymbol{\sigma}$ and the higher-order stresses (or coupled stresses) $\boldsymbol{\tau}$. That is to say, $\boldsymbol{\sigma}:\delta\boldsymbol{\varepsilon}$ and $\boldsymbol{\tau}\vdots\delta\boldsymbol{\eta}$ constitute the work per unit volume of the material for any virtual deformation $\delta\boldsymbol{\varepsilon}$ and virtual deformation gradient $\delta\boldsymbol{\eta}$. Note that $\boldsymbol{\tau}$ is also a third-order tensor symmetric about its first two indices.

Following the conventional limit theorems, an elastic perfectly-plastic constitutive relation is assumed. This relation includes gradients effects and satisfies a generalised yield function of the form:

$$f = f(\sigma_{ij}, \tau_{ijk}) = 0 \tag{2}$$

In Eq. (2), plastic flow can only occur when the stresses satisfy $f = 0$, while $f < 0$ denotes any other state of stress which lies within the elastic range. It is further assumed that the viscosity and inertia effects can be neglected, and that the strain rates and strain gradient rates can be decomposed into elastic and plastic components, respectively, according to:

$$\dot{\varepsilon}_{ij} = \dot{\varepsilon}^{\mathrm{e}}_{ij} + \dot{\varepsilon}^{\mathrm{p}}_{ij}, \quad \dot{\eta}_{ijk} = \dot{\eta}^{\mathrm{e}}_{ijk} + \dot{\eta}^{\mathrm{p}}_{ijk} \tag{3}$$

A generalised form of Hooke's law is assumed to relate the elastic parts $\dot{\varepsilon}^{\mathrm{e}}_{ij}$ and $\dot{\eta}^{\mathrm{e}}_{ijk}$ to the Cauchy stress rates and higher-order stress rates so that:

$$\dot{\sigma}_{ij} = D_{ijkl}\dot{\varepsilon}^{\mathrm{e}}_{kl}, \quad \dot{\tau}_{ijk} = M_{ijkpqr}\dot{\eta}^{\mathrm{e}}_{pqr} \tag{4}$$

where D_{ijkl} and M_{ijkpqr} are, respectively, the conventional elastic stiffness and higher-order elastic stiffness tensors. For an isotropic linear material that will be treated in this paper, Eq. (4) is assumed to have the same form as that proposed by Mindlin (1965) (see also Appendix A). The gradient-dependent constitutive relations are assumed to be analogous to the conventional elastic perfectly-plastic relations, so that both the first order and higher order stress–strain relations are elastic perfectly-plastic. For a sample in simple tension, Fig. 1 shows the stress–strain and higher order stress–strain gradient relations.

2.2. Rephrasing of stability criterion, normality rule and rate of dissipation

In the presence of gradient terms, the stability criterion, normality rule and characteristics of the rate of the dissipation function (see, Drucker et al., 1952) have to be rephrased. First, the Drucker stability criterion requires the gradient-dependent material to satisfy the following conditions:

$$\dot{\sigma}_{ij}\dot{\varepsilon}^{\mathrm{p}}_{ij} + \dot{\tau}_{ijk}\dot{\eta}^{\mathrm{p}}_{ijk} \geqslant 0 \tag{5}$$

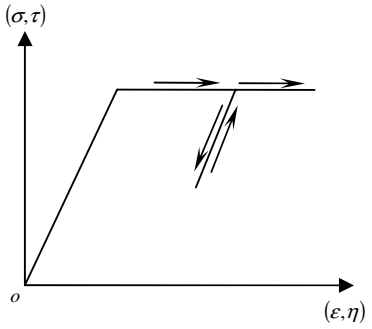

Fig. 1. Schematic constitutive relations of gradient-dependent elastic perfectly plasticity in simple tension.

When defining the normality rule, it is assumed that the plastic strain rates and the plastic strain gradient rates are both related to the stress state. The yield condition $f = 0$ presents a convex surface in the compound stress space of Cauchy and higher-order stresses. Suppose the normality law applies and now consider a stress point $(\sigma_{ij}, \tau_{ijk})$ which satisfies $f = 0$. Any plastic rates for the strains and strain gradients, $(\dot{\varepsilon}^{\mathrm{p}}_{ij}, \dot{\eta}^{\mathrm{p}}_{ijk})$, associated with this stress state may be represented by a ray which lies in the outward normal direction to the yield surface at the point $(\sigma_{ij}, \tau_{ijk})$. In view of this, the following relations immediately hold:

$$\dot{\sigma}_{ij}\dot{\varepsilon}^{\mathrm{p}}_{ij} = 0, \quad \dot{\tau}_{ijk}\dot{\eta}^{\mathrm{p}}_{ijk} = 0 \tag{6}$$

It is further assumed that a homogeneous function $\hat{\Phi}$ exists such that the power dissipation during plastic flow is $\hat{\Phi}(\dot{\varepsilon}^{\mathrm{p}}_{ij}, \dot{\eta}^{\mathrm{p}}_{ijk})$ and for any safe state of stress $(\sigma^{s}_{ij}, \tau^{s}_{ijk})$,

$$(\sigma^{s}_{ij}\dot{\varepsilon}^{\mathrm{p}}_{ij} + \tau^{s}_{ijk}\dot{\eta}^{\mathrm{p}}_{ijk}) < \hat{\Phi}(\dot{\varepsilon}^{\mathrm{p}}_{ij}, \dot{\eta}^{\mathrm{p}}_{ijk}) \tag{7}$$

Here we use the hat symbol '^' over Φ to emphasise that a total dissipation potential for Φ might not exist as $\hat{\Phi}$ can be non-integrable over time in some cases, for instance, where it is path-dependent. It is further supposed that the Cauchy stress σ_{ij} and the higher-order stress τ_{ijk} are homogeneous of order zero in, respectively, the components of the plastic strain rate and the plastic strain gradient rate. There is no dependence of σ_{ij} on $\dot{\eta}^{\mathrm{p}}_{ijk}$, nor τ_{ijk} on $\dot{\varepsilon}^{\mathrm{p}}_{ij}$. Then the sum $(\sigma^{s}_{ij}\dot{\varepsilon}^{\mathrm{p}}_{ij} + \tau^{s}_{ijk}\dot{\eta}^{\mathrm{p}}_{ijk})$ is homogeneous of the first order in the compound space of the components of plastic strain and strain gradients rates. As a result, at a compound stress point $(\sigma_{ij}, \tau_{ijk})$, the following conjugate relations will hold:

$$\dot{\varepsilon}^{\mathrm{p}}_{ij} = \hat{\lambda}\frac{\partial f}{\partial \sigma_{ij}}, \quad \dot{\eta}^{\mathrm{p}}_{ijk} = \hat{\lambda}\frac{\partial f}{\partial \tau_{ijk}} \quad \text{for } f(\sigma_{ij}, \tau_{ijk}) = 0 \tag{8}$$

where $\hat{\lambda}$ is a non-negative multiplier. The reason for using the symbol '^' instead of a dot for $\hat{\lambda}$ is the same as mentioned before for $\hat{\Phi}$.

In general, the dissipative stress space is different from the true stress space (see Collins, 2005). However, if the two spaces coincide with each other, we may interpret the dissipation stresses as being identical to the true stresses during the yielding of the material. In this case, provided Eq. (8) holds, the rate of dissipation function takes the following form:

$$\hat{\Phi} = \sigma_{ij}\dot{\varepsilon}^{\mathrm{p}}_{ij} + \tau_{ijk}\dot{\eta}^{\mathrm{p}}_{ijk} \tag{9}$$

If the yield function defined in Eq. (2) is strictly convex, the Cauchy stress σ_{ij} and higher-order stress τ_{ijk} can be uniquely determined for a given $(\dot{\varepsilon}^{\mathrm{p}}_{ij}, \dot{\eta}^{\mathrm{p}}_{ijk})$. For a yield surface with corners or flat faces this uniqueness is lost, but the rate of dissipation $\hat{\Phi} = \sigma_{ij}\dot{\varepsilon}^{\mathrm{p}}_{ij} + \tau_{ijk}\dot{\eta}^{\mathrm{p}}_{ijk}$ can still be uniquely determined (Chen and Han, 1988).

2.3. Mathematical characterisation of collapse with gradient effects

As stated in Section 1, the physical definition of collapse for a gradient-dependent material remains the same as for a conventional material. The mathematical description of collapse, however, requires some modifications. Consider a gradient-dependent material with volume V and surface S (as is depicted in Fig. 2).

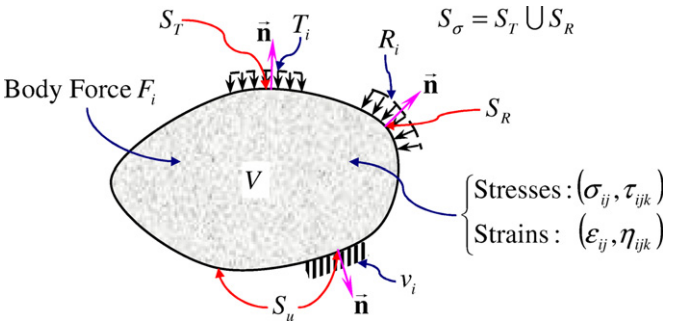

Fig. 2. Boundary conditions for a gradient-dependent material body.

Suppose the velocities are denoted by v_i and the velocity gradients by $v_{i,j}$, while the surface tractions are T_i and the higher-order surface tractions (double tractions) are R_i. Let the body forces be denoted by F_i, with higher-order body forces being neglected in this analysis. The external surface S of V may be divided into two parts: S_σ for static forces and S_u for variable forces. In classical continuum theories, these two boundaries are usually subject to prescribed tractions and velocities, respectively. Due to the introduction of the strain gradients and the higher-order stress terms, extra conditions are required for both S_σ and S_u. The static force surface S_σ is further divided into two portions: S_T for the part which is subject to conventional traction forces and S_R for the part which is subject to higher-order traction forces. Meanwhile, on the kinematic surface S_u, not all components of $v_{i,j}$ are independent of v_i because, for a known v_i, its surface gradient is also known. Hence, a total of six independent displacement boundary conditions are generally required: e.g., the velocities v_i, $i = 1, 2, 3$ as well as their normal gradients along S_u should be prescribed (see, also, Zhao et al., 2005). This is equivalent to the following expression:

$$v_k = v_k^0, \quad n_l \partial_l v_k = \dot{e}_k^0 \quad \text{on } S_u \tag{10}$$

where n_l is the unit outward normal vector on the surface S_u, and $\partial_l v_k$ denotes the surface differentials of the velocities which can be further decomposed into normal and tangential parts:

$$\partial_l v_k = n_l n_i \partial_i v_k + (\delta_{li} - n_l n_i)\partial_i v_k \tag{11}$$

Let

$$D = n_k \partial_k, \quad D_i = (\delta_{ik} - n_i n_k)\partial_k \tag{12}$$

where D denotes the normal differential, the unit normal vector n_k is expressed in local coordinates, and D_i is the surface gradient operator. Eq. (11) may then be rewritten as:

$$\partial_i v_j = n_i D v_j + D_i v_j \tag{13}$$

During the state of collapse, denoted by the superscript 'c', the applied load is assumed to be constant so that the rates $\dot{F}_i^c$ vanish throughout V. The rates of surface tractions and coupled tractions, prescribed as $\dot{T}_i^c$ and $\dot{R}_i^c$, will also vanish, as do the surface velocities v_i^c and their outward-normal gradients due to the definition of the stress and higher order stress boundary conditions. Consequently, the following expressions hold

$$\int_s (\dot{T}_i^c v_i^c + \dot{R}_i^c D v_i^c)\, \mathrm{d}S = 0, \text{ and } \dot{F}_i^c = 0 \quad \text{for some } v_i^c \neq 0 \text{ and } D v_i^c \neq 0 \tag{14}$$

where the normal differential operator D is defined in Eq. (12).

In addition, the rate at which work is done for the gradient-dependent material during collapse may also be derived. If the velocities v_i^c are continuous and have continuous second-order derivatives, which enable the existence of strains and strain gradients in the field, the principle of virtual work yields the following equation:

$$\int_s (T_i^c v_i^c + R_i^c n_k \partial_k v_i^c)\, \mathrm{d}S + \int_V F_i^c v_i^c\, \mathrm{d}V = \int_V (\sigma_{ij}^c \dot{e}_{ij}^c + \tau_{ijk}^c \dot{\eta}_{ijk}^c)\, \mathrm{d}V \tag{15}$$

Note that the strain gradients contribute to the virtual work equation through the surface differentials of the velocities, $\partial_i v_j^c$.

In the above, we have disregarded boundary conditions involving traction rates, velocities and their gradients. This is a consequence of the constant load condition for a collapse state rather than a mere simplification of the problem. As has been defined in the Section 1, a collapse state is one where appreciable changes in the geometry of a structure occur at constant loads. To consider constant loads implies the temporal changes of these loads can be neglected, and all rates and velocities in the problem can thus be disregarded. It is noted, however, that in dealing with practical boundary value problems (BVPs) by either conventional or non-standard theories other than limit theory, such boundary conditions might be important and for some cases even indispensable. In such cases, one needs to correctly identify as many boundary conditions as are necessary to enable the BVP to be properly set up and solved.

2.4. Admissible states and limit theorems for gradient-dependent materials

2.4.1. Statically admissible state and lower bound theorem

For a gradient-dependent material, the Cauchy and higher order stresses, σ_{ij} and τ_{ijk}, are assumed to be continuous functions of the coordinates. A *statically admissible state* with gradient effects is defined as one where the following three conditions are satisfied:

$$\begin{cases} \sigma_{ik,i} - \tau_{ijk,ji} + F_k = 0 & \text{(a)} \\ n_i(\sigma_{ik} - \partial_j \tau_{ijk}) - D_j(n_i \tau_{ijk}) + n_i n_j (D_l n_l)\tau_{ijk} = T_k & \text{(b)} \\ n_i n_j \tau_{ijk} = R_k & \text{(c)} \end{cases} \tag{16}$$

together with the yield criterion (2). Eq. (16a) states the conditions of equilibrium, while the other two equations reflect the boundary conditions for the surface tractions and higher order tractions, respectively. A detailed derivation of these three equations may be found in Zhao et al. (2005). Note that the second equation applies to S_T where the components T_i of the surface traction are given, while the third equation applies to S_R where the components of the higher-order traction R_i are specified.

Note that the preceding definitions may be generalised to include stress fields with a finite number of discontinuities. On either side of such a stress discontinuity, the stresses must satisfy Eq. (16a). Moreover, if n_i^{d} denotes the unit vector normal to a discontinuity surface, equilibrium demands that the Cauchy and higher-order stresses defined by:

$$T_k^* = n_i^{\mathrm{d}}(\sigma_{ik} - \partial_j \tau_{ijk}) - D_j(n_i^{\mathrm{d}} \tau_{ijk}) + n_i^{\mathrm{d}} n_j^{\mathrm{d}} (D_l n_l^{\mathrm{d}})\tau_{ijk} \quad \text{and} \quad R_k^* = n_i^{\mathrm{d}} n_j^{\mathrm{d}} \tau_{ijk} \tag{17}$$

must have the same values on either side of the discontinuity (see, e.g., for a shear band, Zhao et al., 2005). Note that the term $\sigma_{ij} n_j^{\mathrm{d}}$, which must be continuous across a stress discontinuity in conventional limit analysis, will not necessarily be continuous in the presence of the strain gradients and higher-order stresses.

As in conventional limit analysis, the lower bound theorem for a gradient-dependent material model follows from the computation of a statically admissible stress state. For a gradient-dependent material undergoing small deformations, a statically admissible stress field is one which satisfies the equilibrium and traction boundary conditions defined in Eq. (16), and nowhere violates the yield criterion (2). Any field of Cauchy and higher-order stresses that satisfies all the conditions of the lower bound theorem is referred to as a statically admissible compound stress field. The load supported by such a stress field gives a lower bound on the collapse load for a gradient-dependent material model. A proof of this gradient-dependent lower-bound theorem is presented in Appendix B.

2.4.2. Kinematically admissible state and upper-bound theorem

A velocity field v_i is said to be kinematically admissible if it satisfies the velocity boundary conditions and the plastic flow rule defined by Eq. (8). Special discontinuous velocity fields are also permissible and useful in certain circumstances. However, here we consider only a kinematically admissible velocity field for which the velocity components are continuous throughout the material. Letting the superscript 'k' denote a kinematically admissible quantity, the strain rates and strain gradient rates are computed from the velocities as:

$$\dot{\varepsilon}_{ij}^{\mathrm{k}} = \frac{1}{2}(v_{i,j}^{\mathrm{k}} + v_{j,i}^{\mathrm{k}}), \quad \dot{\eta}_{ijk}^{\mathrm{k}} = \frac{1}{2}(v_{k,ij}^{\mathrm{k}} + v_{k,ji}^{\mathrm{k}}) \tag{18}$$

If the power expended by the actual surface tractions, higher-order tractions and body forces equals or exceeds the power dissipated by the plastic strains and strain gradient rates in a velocity field, a *kinematically admissible state of collapse* is defined. For such a kinematically admissible collapse state, the following relation holds in analogue to the corresponding conventional theorem (Chen and Han, 1988):

$$\int_s (T_i^{\mathrm{k}} v_i^{\mathrm{k}} + R_i^{\mathrm{k}} D v_i^{\mathrm{k}})\, \mathrm{d}S + \int_V F_i^{\mathrm{k}} v_i^{\mathrm{k}}\, \mathrm{d}V \geqslant \int_V \hat{w}(\dot{\varepsilon}_{ij}^{\mathrm{k}} \dot{\eta}_{ijm}^{\mathrm{k}})\, \mathrm{d}V \tag{19}$$

where the normal differential operator D is defined in Eq. (12) and $\hat{w}(\dot{\varepsilon}^{\mathbf{k}}_{ij}, \dot{\eta}^{\mathbf{k}}_{ijm})$ is a rate of dissipation density which may be expressed in terms of plastic strain rates and plastic strain gradient rates according to:

$$\int_V \hat{w}(\dot{\varepsilon}^{\mathrm{k}}_{ij}\dot{\eta}^{\mathrm{k}}_{ijm})\,\mathrm{d}V = \int_V (\sigma^{\mathrm{k}}_{ij}\dot{\varepsilon}^{\mathrm{k}}_{ij} + \tau^{\mathrm{k}}_{ijm}\dot{\eta}^{\mathrm{k}}_{ijm})\,\mathrm{d}V \tag{20}$$

Again, the reason we use a hat over w here is similar to that for $\hat{\Phi}$ or $\hat{\lambda}$. The left-hand side of inequality (19) defines the external power expended by the surface tractions, higher-order tractions and body forces, while the right-hand side defines the rate of internal power dissipation. Inequality (19) is a statement of the *upper bound theorem* for a gradient-dependent material. It implies that the loads T_i, R_i and F_i, found by equating the external rate of work done to the internal power dissipation, will be not less than the actual limit load. A proof of the above gradient-dependent upper-bound theorem is presented in Appendix C of this paper, in analogue to that for the corresponding conventional theorem by Chen and Han (1988).

2.4.3. Connection with other extremum principles

The statically and kinematically admissible states defined in Sections 2.4.1 and 2.4.2 can be interpreted in terms of related extremum principles. Indeed, the kinematically admissible state defined by Eq. (19) is equivalent to a minimum principle proposed by Smyshlyzev and Fleck (1996) for gradient-dependent materials. This principle states that the 'true' strain energy function W of the material minimises the functional $\widetilde{W}(\dot{\varepsilon}_{ij}, \dot{\eta}_{ijm})$ (or alternatively $\widetilde{W}(v_i)$) for any kinematically admissible field v_i, subject to the boundary conditions defined in Eq. (10). This implies that:

$$\widetilde{W}(v_i) = \int_V \tilde{\hat{w}}(\dot{\varepsilon}_{ij}, \dot{\eta}_{ijk})\,\mathrm{d}V \geqslant W = \int_V \hat{w}(\dot{\varepsilon}^*_{ij}, \dot{\eta}^*_{ijk})\,\mathrm{d}V \tag{21}$$

where $\tilde{\hat{w}}(\dot{\varepsilon}_{ij}, \dot{\eta}_{ijk})$ denotes a kinematically-admissible rate of strain energy density and $\hat{w}(\dot{\varepsilon}^*_{ij}, \dot{\eta}^*_{ijk})$ is the strain energy density for the true velocity field with $(\dot{\varepsilon}^*_{ij}, \dot{\eta}^*_{ijk})$ being defined by the true velocity v^*_i. The proof of this principle follows the standard procedures outlined by Fleck and Hutchinson (1993) or Smyshlyzev and Fleck (1996). A key assumption here is that a convex strain energy function $\widetilde{W}$ exists for any state of strain $(\varepsilon_{ij}, \eta_{ijk})$ generated by external loads on the body. If the true velocity v^*_i is further assumed to correspond to that for a kinematically admissible collapse state, say v^{k}_i, then the theorem expressed in Eq. (19) is equivalent to the minimum principle in Eq. (21).

The theory for a statically admissible state is also connected to the aforementioned minimum principle via a conjugate relation. This takes the form of a complementary minimum principle, expressed in terms of the Cauchy and higher-order stresses, and states that a complementary energy density rate (stress potential) $\hat{\phi}$ may be introduced as a dual to the rate of strain energy density $\hat{w}$ as (Smyshlyzev and Fleck, 1996):

$$\hat{\phi}(\sigma_{ij}, \tau_{ijk}) = \sup_{(\dot{\varepsilon},\dot{\eta})} \{\sigma_{ij}\dot{\varepsilon}_{ij} + \tau_{ijk}\dot{\eta}_{ijk} - \hat{w}(\dot{\varepsilon}_{ij}, \dot{\eta}_{ijk})\} \tag{22}$$

For a smooth and strictly convex function of $\hat{w}$, this complementary energy density rate function is also convex with respect to $(\sigma_{ij}, \tau_{ijk})$. Integrating it over the volume V of the body gives the complementary energy Ψ as:

$$\Psi = \int_V \hat{\phi}(\sigma_{ij}, \tau_{ijk})\,\mathrm{d}V \tag{23}$$

The complementary minimum principal states that, for any stress field $(\sigma_{ij}, \tau_{ijk})$ in V which is statically admissible (i.e. satisfies each of the Eq. (16)), the true complementary energy Ψ^* minimises the functional Ψ in Eq. (22) so that (Smyshlyzev and Fleck, 1996):

$$\Psi^*(\sigma^*_{ij}, \tau^*_{ijk}) \leqslant \Psi(\sigma_{ij}, \tau_{ijk}) \tag{24}$$

This implies that a lower bound collapse load, computed from a statically admissible stress field, corresponds to maximising the true complementary energy Ψ^*.

3. Applications

Analytical lower and upper bound solutions for geotechnical applications are useful not only for practical engineering designs, but also for the calibration of computational limit analyses. This section presents some analytical solutions, based on the preceding gradient-dependent limit theorems, for plane strain conditions. The material behaviour is assumed to be governed by a generalised Drucker–Prager yield criterion.

3.1. Generalised Drucker–Prager criterion for yielding in gradient-dependent materials

A key characteristic of geomaterials is their pressure-dependent plastic yielding. With the presence of higher-order stresses in the gradient-dependent constitutive relations, it is necessary to include these quantities in the yielding behaviour as well. Following Fleck and Hutchinson (1997), the hydrostatic higher-order stress may be defined as a third-order tensor according to:

$$\tau^{\mathrm{h}}_{ijk} = \frac{1}{4}(\delta_{ik}\tau_{jpp} + \delta_{jk}\tau_{ipp}) \tag{25}$$

This relation decomposes the higher-order stress τ_{ijk} into a hydrostatic part τ^{h}_{ijk} and a deviatoric part $\tau'_{ijk} = \tau_{ijk} - \tau^{\mathrm{h}}_{ijk}$, with the latter having the property $\tau'_{ijj} = \tau'_{jij} = 0$. In the case of an incompressible material where $\eta_{ikk} = \eta_{kik} = 0$, the hydrostatic higher-order stress τ^{h}_{ijk} cannot do work so that $\tau^{\mathrm{h}}_{ijk}\eta_{ijk} = 0$. Since τ^{h}_{ijk} is a third-order tensor, it has no simple first invariant other than a quadratic form. Such a quadratic invariant will inevitably introduce more parameters and will not fit well with the first invariant of σ_{kk} if the two are combined to give the total hydrostatic component of the stresses. In view of these complications, we choose not to decompose the higher-order stress in this way. Instead, the higher-order stresses are assumed to contribute to the equivalent deviatoric stresses in a simplified manner, and not augment the hydrostatic stresses at all. This assumption, which is made purely for the sake of convenience, leads to the following generalised Drucker–Prager criterion for a gradient-dependent material:

$$f = \alpha I_1 + J_2^{1/2} - k = 0 \tag{26}$$

In the above, α and k are material constants which are similar to those in the conventional Drucker–Prager criterion, and

$$I_1 = \sigma_{kk} \tag{27}$$

$$J_2 = (s_{ij}s_{ij} + l^{-2}\tau_{ijk}\tau_{ijk})/2 \tag{28}$$

In Eq. (28), l denotes an internal length scale resulting from the introduction of strain gradients and $s_{ij} = \sigma_{ij} - \sigma_{kk}\delta_{ij}/3$ denotes the usual deviatoric part of the Cauchy stress. Note that the higher-order stresses do not contribute to the hydrostatic invariant I_1, and appear in the modified deviatoric invariant J_2 through a quadratic form which is similar to that for s_{ij}.

Applying the normality rule (8) to the yield criterion (26) results in the following plastic strain rates and plastic strain gradient rates:

$$\dot{\varepsilon}^{\mathrm{p}}_{ij} = \hat{\lambda}[\alpha\delta_{ij} + s_{ij}/2J_2^{1/2}], \quad \dot{\eta}^{\mathrm{p}}_{ijk} = \hat{\lambda}l^{-2}\tau_{ijk}/2J_2^{1/2} \tag{29}$$

The plastic volumetric strain rate for our gradient-dependent material is the same as that for the standard Drucker–Prager criterion:

$$\dot{\varepsilon}^{\mathrm{p}}_{v} = \dot{\varepsilon}^{\mathrm{p}}_{ii} = 3\alpha\hat{\lambda} \tag{30}$$

As with the conventional Drucker–Prager criterion, Eq. (30) predicts dilatancy for a point undergoing plastic yielding when $\alpha > 0$. Indeed, the coefficient α still acts as a measure of plastic volume dilatation for the gradient-dependent material. Clearly the plastic volumetric strain rate would be different from (30) if the first invariant I_1 was assumed to depend on the hydrostatic part of the higher-order stress tensor.

It is also useful to derive the rate of plastic dissipation associated with the generalised Drucker–Prager criterion when plastic yielding occurs in the material. Using Eqs. (9), (26) and (29), the power dissipation per unit volume may be obtained as:

$$\hat{\Phi} = \hat{\lambda}[\alpha I_1 + \sqrt{J_2}] = \hat{\lambda} k \tag{31}$$

From (29) we have:

$$\sqrt{\dot{\varepsilon}^{\mathrm{p}}_{ij}\dot{\varepsilon}^{\mathrm{p}}_{ij} + l^2 \dot{\eta}^{\mathrm{p}}_{ijk}\dot{\eta}^{\mathrm{p}}_{ijk}} = \frac{\hat{\lambda}}{2}\sqrt{12\alpha^2 + 2} \tag{32}$$

and the power dissipation per unit volume for the gradient-dependent Drucker–Prager material is:

$$\hat{\Phi} = \frac{2k\sqrt{\dot{\varepsilon}^{\mathrm{p}}_{ij}\dot{\varepsilon}^{\mathrm{p}}_{ij} + l^2 \dot{\eta}^{\mathrm{p}}_{ijk}\dot{\eta}^{\mathrm{p}}_{ijk}}}{\sqrt{12\alpha^2 + 2}} \tag{33}$$

When the gradient terms are dropped, we immediately recover the power dissipation for the conventional Drucker–Prager criterion according to:

$$\hat{\Phi}^0 = \frac{2k\sqrt{\dot{\varepsilon}^{\mathrm{p}}_{ij}\dot{\varepsilon}^{\mathrm{p}}_{ij}}}{\sqrt{12\alpha^2 + 2}} \tag{34}$$

Note further that, if $\alpha = 0$, a generalised von Mises (or Prandtl–Reuss) criterion is obtained from Eq. (26):

$$f = J_2^{1/2} - k = 0 \tag{35}$$

and frictional effects in equations from (31) to (34) are neglected. For this case the power dissipation takes the simple form of $\hat{\Phi} = k\sqrt{2\dot{\varepsilon}^{\mathrm{p}}_{ij}\dot{\varepsilon}^{\mathrm{p}}_{ij} + 2l^2\dot{\eta}^{\mathrm{p}}_{ijk}\dot{\eta}^{\mathrm{p}}_{ijk}}$.

3.2. Generalised plane strain problems

A *generalised plane strain state* for strain gradient theory assumes that both the strains and strain gradients are zero in one of the Cartesian coordinate directions (say, in the x_3 direction). Thus, the following terms will vanish:

$$\begin{cases} \dot{\varepsilon}_{i3} = \dot{\varepsilon}_{3i} = 0 \\ \dot{\eta}_{ij3} = \dot{\eta}_{i3j} = \dot{\eta}_{3ij} = 0 \end{cases} \tag{36}$$

where $i = 1,2,3$, and $j = 1,2,3$. Consequently, the non-zero strains and strain gradients for the generalised plane strain state are $\dot{\varepsilon}_{11}, \dot{\varepsilon}_{12} = \dot{\varepsilon}_{21}, \dot{\varepsilon}_{22}$, $\dot{\eta}_{111}, \dot{\eta}_{112}, \dot{\eta}_{121} = \dot{\eta}_{211}, \dot{\eta}_{122} = \dot{\eta}_{212}, \dot{\eta}_{221}, \dot{\eta}_{222}$. The corresponding stress state depends on the particular problem to be addressed. In the following subsections, we develop analytical lower and upper bound solutions for the collapse of a gradient-dependent layer, subjected to simple shear and uniaxial compression conditions.

3.3. Simple shear deformation of a gradient-dependent layer

3.3.1. Lower bound for the shear force

Consider a gradient-dependent layer under plane strain simple shear conditions, as shown in Fig. 3. Let the height of the layer be h, the shear stress applied to the ends be T^0, and the coordinate system be fixed so that the x-axis and y-axis divide the layer into two even halves. The width of the layer is not specified, with the possibility of it varying between a finite value and infinity, and it is assumed that neither higher-order surface tractions nor body forces present. To derive a lower bound on the applied shear stress, we first consider the statically admissible state where there is no yielding, as shown in Fig. 3a. As no plastic dilation occurs, we assume the vertical displacement is zero and the horizontal displacement is purely a function of y so that $u_1 = u(y) \neq 0$. Letting $\gamma = \partial u/\partial y$ denote the engineering shear strain, the non-zero strain and strain gradient components are $\varepsilon_{21} = \varepsilon_{12} = \gamma/2$ and $\eta_{221} = \gamma_{,2}/2$.

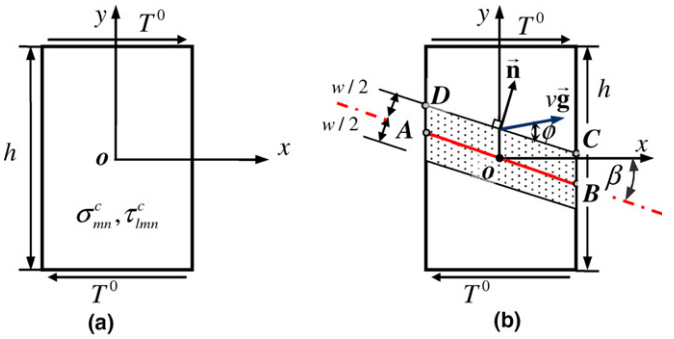

Fig. 3. Simple shear of a gradient-dependent von Misses layer: (a) statically admissible state, where σ^c_{mn} denote σ^c_{21} and σ^c_{21}, and τ^c_{lmn} denote τ^c_{111}, τ^c_{112}, τ^c_{113}, τ^c_{221}, $\tau^c_{212}, \tau^c_{331}$ and τ^c_{313}; (b) kinematically admissible state.

If we further assume the material is isotropic, then the elastic relations may be characterised by the second and third order formulations developed by Mindlin (1965) (see Appendix A). Consequently, the non-zero Cauchy stresses in the layer are σ_{21} and σ_{12} with $\sigma_{21} = \sigma_{12}$, while there are seven non-zero components for the higher-order stresses: $\tau_{111}, \tau_{122}, \tau_{133}, \tau_{221}, \tau_{212}, \tau_{331}, \tau_{313}$. All seven of the latter are linear functions of the strain gradient η_{221}. The elastic relations for σ_{21} and τ_{221} are thus:

$$\begin{cases} \sigma_{21} = 2\mu_1\varepsilon_{21}, \quad \tau_{221} = 2l^2\mu_2\eta_{221} \\ \tau_{111} = \xi_1\tau_{221}, \quad \tau_{122} = \tau_{212} = \xi_2\tau_{221}, \quad \tau_{133} = \tau_{313} = \xi_3\tau_{221}, \quad \tau_{331} = \xi_4\tau_{221} \end{cases} \tag{37}$$

where μ_1 is the conventional shear modulus, μ_2 may be regarded as a generalised shear modulus for the gradient terms, and both quantities have the unit of stress (Mindlin, 1965). The constants ξ_i, $(i = 1, \ldots, 4)$ denote the ratio of the shear modulus of the corresponding component to that of τ_{221}. For the sake of simplicity, we assume $a_1 = a_2 = a_3 = a_4 = a_5$ in Eq. (A.2) for this simple shear problem, which implies the five means of strain gradient combinations on the right side of Eq. (A.2) contribute equally to the higher order stresses. In this case, we have

$$\xi_1 = \frac{3}{4}, \quad \xi_2 = \frac{1}{8}, \quad \xi_3 = \frac{1}{8}, \quad \xi_4 = \frac{1}{2} \tag{38}$$

In Eq. (37), the ratio μ_1/μ_2 may be viewed as an index which reflects the impact of gradient effects on the overall response. The higher this value is, the less significant the gradient effects will be. When $\mu_2 = 0$ (and thus $\mu_1/\mu_2 = \infty$), the gradient effects are completely neglected and conventional first order mechanics prevails. This may be verified in the numerical results to be derived.

A gradient-dependent lower bound on the shear force T^0 will be derived first. Consider the statically admissible state shown in Fig. 3a. The equilibrium equations (16a) for simple shear give:

$$\sigma_{21,2} - \tau_{111,11} - \tau_{221,22} - \tau_{331,33} = 0 \tag{39}$$

Noting that $\eta_{221,11} = \eta_{221,33} = 0$, $\tau_{111} = 2\xi_1 l^2\mu_2\eta_{221}$ and $\tau_{331} = 2\xi_4 l^2\mu_2\eta_{221}$, we have: $\tau_{111,11} = \tau_{331,33} = 0$ and the above equation is simplified to:

$$\sigma_{21,2} - \tau_{221,22} = 0 \tag{40}$$

Integration of this equation over the interval $y = [0, h/2]$ results in:

$$\sigma_{21} - \tau_{221,2} = T^0 \tag{41}$$

As there is still a partial differential in Eq. (41), it is difficult to determine σ_{21} and σ_{221} from Eq. (41) directly. Employing a virtual displacement field with $u_1 = u(y) \neq 0$ and a constant shear strain γ, and substituting (37) in (41), lead to

$$\mu_1\gamma - l^2\mu_2\gamma_{,22} = T^0 \tag{42}$$

The general solution to this ordinary differential equation is:

$$\gamma = \frac{T^0}{\mu_1} + C_1 \exp\left(\frac{y}{l}\sqrt{\frac{\mu_1}{\mu_2}}\right) + C_2 \exp\left(-\frac{y}{l}\sqrt{\frac{\mu_1}{\mu_2}}\right) \tag{43}$$

where C_1 and C_2 are unknown constants which can be found from symmetry and the boundary conditions described in Eq. (16b) and (16c). In the case of simple shear, as shown in Fig. 3a, the shear strain is anti-symmetric so that $\gamma|_{y=0} = 0$. Applying this condition to Eq. (43) gives:

$$C_1 + C_2 = -T^0/\mu_1 \tag{44}$$

Since we have assumed no higher-order surface tractions exist on the surface $y = h/2$, Eq. (16c) yields:

$$R_1|_{y=h/2} = n_2 n_2 \tau_{221}|_{y=h/2} = 0 \tag{45}$$

Noting that $n_2 n_2 = 1$ on the surface $y = h/2$, we obtain:

$$\tau_{221}|_{y=h/2} = 0 \tag{46}$$

Combining Eqs. (37), (43) and (46) gives:

$$C_2 = C_1 \exp\left(\frac{h}{l}\sqrt{\frac{\mu_1}{\mu_2}}\right) \tag{47}$$

which, after insertion into (44), leads to:

$$C_1 = -T^0 \Big/ \mu_1\left(1 + \exp\left(\frac{h}{l}\sqrt{\frac{\mu_1}{\mu_2}}\right)\right), \quad C_2 = -T^0 \Big/ \mu_1\left(1 + \exp\left(-\frac{h}{l}\sqrt{\frac{\mu_1}{\mu_2}}\right)\right) \tag{48}$$

Hence the virtual shear strain is:

$$\gamma = \frac{T^0}{\mu_1}\left(1 - \frac{\exp\left(\frac{y}{l}\sqrt{\frac{\mu_1}{\mu_2}}\right)}{1 + \exp\left(\frac{h}{l}\sqrt{\frac{\mu_1}{\mu_2}}\right)} - \frac{\exp\left(-\frac{y}{l}\sqrt{\frac{\mu_1}{\mu_2}}\right)}{1 + \exp\left(-\frac{h}{l}\sqrt{\frac{\mu_1}{\mu_2}}\right)}\right) \tag{49}$$

For the statically admissible state, we concerned only with stresses. Using Eqs. (37) and (49), the following normalised shear stress and higher-order shear stress relations are obtained:

$$\frac{\sigma_{21}}{T^0} = \left(1 - \frac{\exp\left(\frac{y}{l}\sqrt{\frac{\mu_1}{\mu_2}}\right)}{1 + \exp\left(\frac{h}{l}\sqrt{\frac{\mu_1}{\mu_2}}\right)} - \frac{\exp\left(-\frac{y}{l}\sqrt{\frac{\mu_1}{\mu_2}}\right)}{1 + \exp\left(-\frac{h}{l}\sqrt{\frac{\mu_1}{\mu_2}}\right)}\right) \tag{50}$$

$$\frac{\tau_{221}}{lT^0} = \sqrt{\frac{\mu_2}{\mu_1}}\left(\frac{\exp\left(-\frac{y}{l}\sqrt{\frac{\mu_1}{\mu_2}}\right)}{1 + \exp\left(-\frac{h}{l}\sqrt{\frac{\mu_1}{\mu_2}}\right)} - \frac{\exp\left(\frac{y}{l}\sqrt{\frac{\mu_1}{\mu_2}}\right)}{1 + \exp\left(\frac{h}{l}\sqrt{\frac{\mu_1}{\mu_2}}\right)}\right) \tag{51}$$

All other non-zero higher-order stresses follow immediately from Eqs. (37) and (51).

The distributions of σ_{21} and τ_{221} along the positive y direction are shown in Fig. 4. The ratio between the layer height and the internal length scale, h/l, is assumed to be 100, while five sets of the ratio μ_1/μ_2 are used to investigate the influence of the gradient effects. Fig. 4a shows that σ_{21} exhibits a zero value at the center of the layer ($y = 0$) and, as expected, gradually increases to the boundary traction value T^0 when approaching the top surface ($y = h/2$). In contrast, Fig. 4b indicates that τ_{221} generally has its largest value at the center of the layer ($y = 0$), and then gradually reduces to zero when approaching the end ($y = h/2$). The influence of μ_1/μ_2 on the distribution of both σ_{21} and τ_{221} is marked, with lower values for μ_1/μ_2 implying larger gradient effects on the overall mechanical response. Smaller values of μ_1/μ_2 cause σ_{21} to reach its peak value at larger values

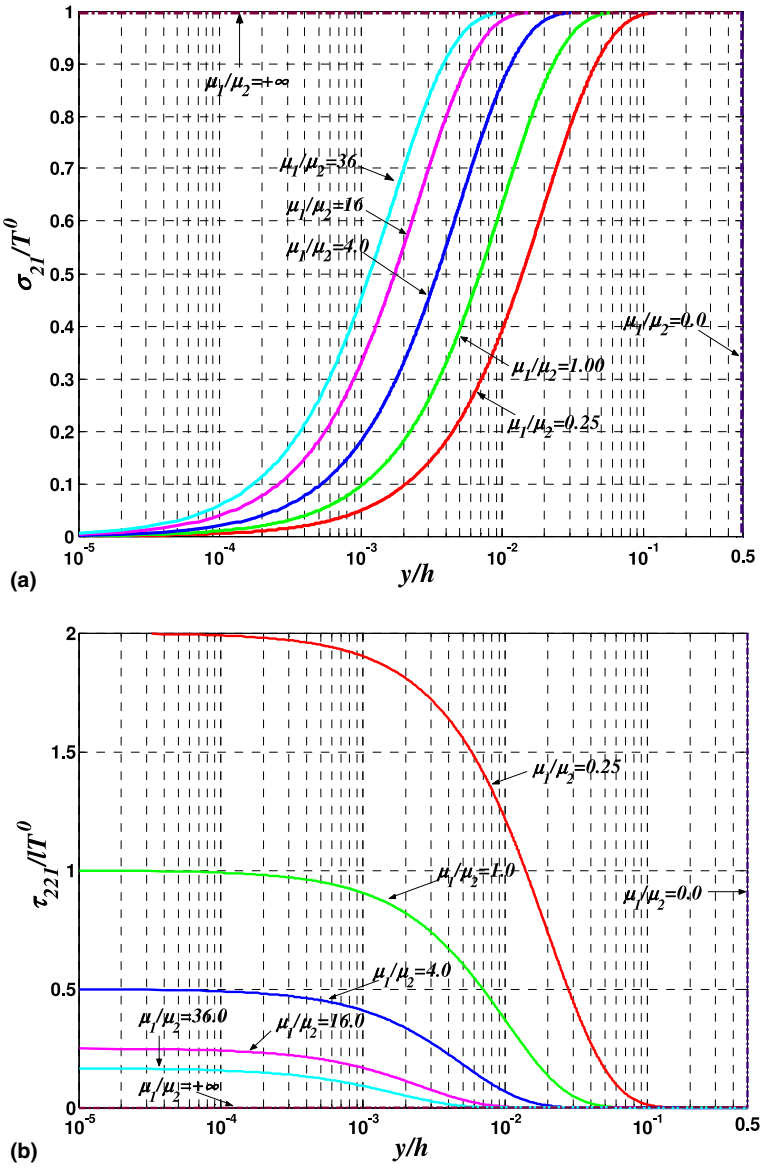

Fig. 4. Normalised distribution profile for σ_{21} and τ_{221} along $y = [0, h/2]$ ($h/l = 100$): (a) σ_{21}/T^0 vs. y/h; (b) τ_{221}/lT^0 vs. y/h.

of y. The two extreme cases, $\mu_1/\mu_2 = 0$ and $\mu_1/\mu_2 = +\infty$, give $\sigma_{21} = 0$ and $\sigma_{21} = T^0$ throughout the profile, respectively, while the corresponding τ_{221} values are $\tau_{221} = \infty$ and $\tau_{221} = 0$. These two cases thus correspond to total gradient theory (where the Cauchy stresses are zero) and conventional solid mechanics theory (where the gradient stresses are zero). In conjunction with the variation of μ_1/μ_2, the behaviour of σ_{21} at $y = h/2$ and τ_{221} at $y = 0$ ultimately determine the lower bound. Note that the distributions for all other non-zero higher-order stress components are similar to that for τ_{221}, and will not be shown here.

A lower bound on T^0 for the simple shear problem, T^0_{L}, requires the Cauchy and higher-order stresses at every point in the layer to satisfy the statically admissible conditions (16) and the yielding criterion (26). For a stress field which satisfies (16), this is equivalent to the following statement:

$$T^0_{\mathrm{L}} = \inf_{(\sigma,\tau,y)} \{(\sigma_{ab}, \tau_{abc}, y) :\to \max[f^0(\sigma_{ab}, \tau_{abc}, y) = \alpha I_1 + J_2^{1/2}] \text{ and } f^0 = k\} \tag{52}$$

where σ_{ab} and τ_{abc} denote, respectively, the non-vanishing stresses and higher-order stresses in the layer under simple shear, e.g., σ_{21}, σ_{12}, τ_{111}, τ_{122}, τ_{133}, τ_{221}, τ_{212}, τ_{331} and τ_{313}. As for this special case of simple shear, the hydrostatic stress and generalised deviatoric stress defined in Eqs. (27) and (28) are respectively:

$$I_1 = 0, \quad J_2 = (2\sigma_{21}^2 + l^{-2}\zeta\tau_{221}^2)/2 \tag{53}$$

where $\zeta = 1 + \xi_1^2 + 2\xi_2^2 + 2\xi_3^2 + \xi_4^2$. Thus the yield function (26) can be further simplified to the following form:

$$f = \sqrt{(2\sigma_{21}^2 + l^{-2}\zeta\tau_{221}^2)/2} - k = 0 \tag{54}$$

The maximisation problem (52) can be solved by substituting Eqs. (50) and (51) into Eq. (54), and then finding a point in the layer, y_m, that maximises $f^0 = \sqrt{(2\sigma_{21}^2 + l^{-2}\zeta\tau_{221}^2)/2}$. Once this point is known, the corresponding values of σ_{21} and τ_{221} at y_m can be found and inserted into Eq. (54) to solve the equation for T^0. Because of the dependence of f^0 on ξ_i, μ_1/μ_2 and h/l, a general solution for the maximum of f^0 cannot be found easily. Let us assume that ξ_i $(i = 1, \ldots, 4)$ have the values defined in (38) so that $\zeta = 15/8$ in (53). For this case, the maximum of f^0 occurs either at $y_m = 0$ or at $y_m = h/2$. Following the above procedure, a lower bound on the shear force T^0 for the former case is:

$$T_{\mathrm{L}}^0 \geqslant T^0 = \sqrt{\frac{\mu_1}{\mu_2}}\left(\frac{\exp\left(\frac{h}{l}\sqrt{\frac{\mu_1}{\mu_2}}\right) + 1}{\exp\left(\frac{h}{l}\sqrt{\frac{\mu_1}{\mu_2}}\right) - 1}\right)\frac{k}{\sqrt{\zeta/2}} \tag{55}$$

When f^0 is a maximum at $y_m = h/2$, we obtain:

$$T_{\mathrm{L}}^0 \geqslant T^0 = \frac{\exp\left(\frac{h}{l}\sqrt{\frac{\mu_1}{\mu_2}}\right) + 1}{\left(\exp\left(\frac{h}{2l}\sqrt{\frac{\mu_1}{\mu_2}}\right) - 1\right)^2}k \tag{56}$$

Once μ_1/μ_2 and h/l are fixed for a particular material layer under simple shear, the lower bound is determined by either Eq. (55) or (56). For a fixed value of h/l, there is a threshold quantity r_c so that when $\mu_1/\mu_2 < r_c$ the lower bound is given by (55). The precise value of r_c may be obtained by equating the two bounds from (55) and (56). For h/l equal to 2, 4, 8, 10 and 100, the respective values of r_c are 2.2931, 1.3764, 1.0077, 0.9655 and 0.9375. Once $h/l \geqslant 100$, the value of r_c remains approximately constant. The bound given by Eq. (56) corresponds to the case where conventional terms dominate and the gradient terms are negligible, whereas Eq. (55) implies the opposite case. For a simply sheared layer with specified h/l, this implies that the threshold r_c marks the zone of influence of the conventional and gradient terms on the lower bound. The lower bounds obtained above are plotted in another way in Fig. 5 for cases where $h/l = 2$, 4, 10 and 100. In all instances the lower bound T_{L}^0 exhibits a maximum value at the threshold $\mu_1/\mu_2 = r_c$, and decreases as the ratio μ_1/μ_2 decreases. Above the threshold r_c the lower bound still decreases with increasing μ_1/μ_2 until, when μ_1/μ_2 is large enough, it approximates k. It is easy to verify that, if gradient effects are neglected, the lower bound on the shear force from conventional mechanics theory is:

$$T_{\mathrm{LC}}^0 = k \tag{57}$$

This result can be obtained immediately by setting $\mu_1/\mu_2 = +\infty$ in Eq. (56).

The influence of h/l on T_{L}^0 is of key importance. Fig. 5 shows that when h/l is small, say $h/l = 2$, the shear force is applied to a layer comprising two vertically arranged grains or microstructures. In this case the gradient effects on the lower bound T_{L}^0 are appreciable, even when μ_1/μ_2 is relatively large. For larger values of h/l, the gradient effects are not so significant and the predicted value of T_{L}^0 is similar to the conventional solution once $\mu_1/\mu_2 \geqslant r_c$. Regardless of the value of μ_1/μ_2, smaller values of h/l lead to a larger prediction for T_{L}^0. As shown in Fig. 5, a peak bound of 1.72 times the conventional bound is predicted for $h/l = 2$. These results can be used to explain the phenomenon of size effects in material strength. When h/l is large, the effects of microstructure (represented by the internal length scale l) may be neglected, as the strength is dominated by

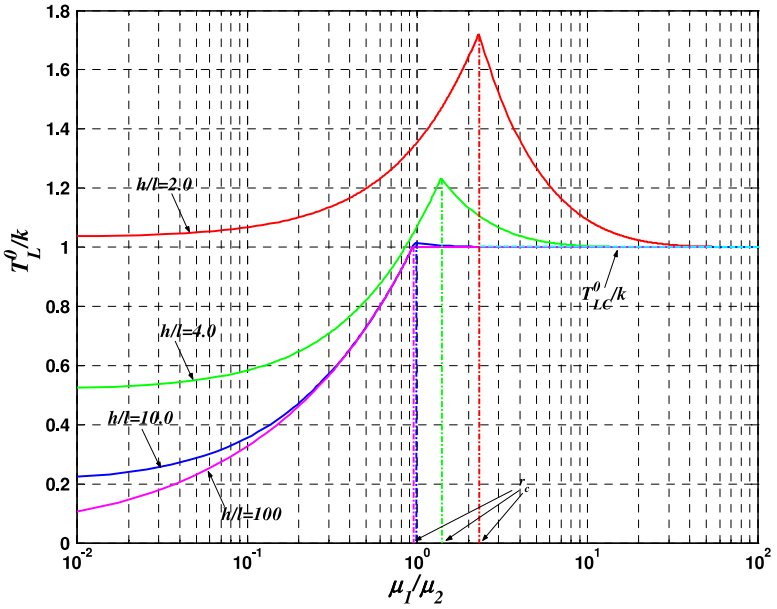

Fig. 5. Influence of μ_1/μ_2 and h/l on the gradient-dependent lower bound shear force T^0_{L} for simple shear.

macroscopic effects (the sample size h). The gradient effects are thus insignificant and the material strength (here the predicted lower bound) is relatively low. However, when h/l is small, so that the microstructural dimensions are comparable with the macroscopic size, the gradient terms play an important role in sustaining the applied load, and the observed material strength will generally be higher. It is also of interest to discuss the left branch of the gradient-dependent lower bound solution. As mentioned above, when the ratio μ_1/μ_2 becomes extremely small, the predicted T^0_{L} becomes small as well. In cases other than $h/l = 2$, T^0_{L} is even smaller than k. This behaviour implies that, whenever the conventional terms are insignificant, the gradient effects can only sustain a smaller load, unless the sample size is comparable with the microstructural length. This conclusion, however, is not universal and only applicable to the simple shear problem where the higher-order boundary traction is assumed to be absent. For a real material, the mechanical behaviour will not necessarily be isotropic and linear elastic. In such a case, the ratio μ_1/μ_2 may depend not only on the material, but also on the sample size and the stress level. Further studies will be required to calibrate this type of behaviour quantitatively.

3.3.2. A gradient-dependent upper bound for the shear force T^0

In this subsection, an upper bound for the gradient-dependent layer subjected to simple shear will be sought. A compatible collapse mechanism is assumed, as illustrated in Fig. 3b. A shear band is assumed to form with an angle of β to the x direction, where β is to be determined. The Cartesian origin O is the geometric center of the sample as in Fig. 3a. When the shear band is fully developed to a width of w, a slip line is assumed to occur along its centerline AOB. Along this slip line, the upper endpiece of the sample above the shear band moves as a rigid body in the opposite direction to the lower portion. The velocity above the shear band CD is assumed to be v. To accommodate plastic dilation within the band, the direction of the velocity is assumed to be inclined at an angle ϕ to CD. This ϕ is the friction angle for the gradient-dependent material characterised by the generalised Drucker–Prager criterion in Eq. (26), and is assumed to have the same relation to the coefficient α as derived by Drucker and Prager (1952):

$$\phi = \cos^{-1}\left(\frac{\sqrt{1-12\alpha^2}}{\sqrt{1-3\alpha^2}}\right) \tag{58}$$

It is easily shown that physically meaningful values for α must lie in the range $[0, 1/\sqrt{12}]$. According to Fig. 3b, the outward unit-normal of the shear band, $\vec{\mathbf{n}}$, and the unit directional vector of the velocity of the upper end-piece, $\vec{\mathbf{g}}$, respectively, are:

$$\vec{\mathbf{n}} = (n_1, n_2) = (\sin\beta, \cos\beta), \quad \vec{\mathbf{g}} = (g_1, g_2) = (\cos(\phi - \beta), \sin(\phi - \beta)) \tag{59}$$

Within the band, it is further assumed that the velocity varies linearly from one boundary to the other. Then at the slip line, the absolute velocity is zero. A homogeneous deformation within the band may thus be assumed. Note that the afore-assumed collapse mechanism is similar to that outlined by Hill (2001) for localised necking analysis. However, we here also consider plastic flow with gradient effects in the shear band. Furthermore, for simplicity, we neglect all the anisotropy that may exist or be induced during the deformation. Consider now the upper half of the sample. In relation to the above assumptions, it is straightforward to verify that the following relations hold for each point in the parallelogram $ABCD$:

$$\frac{\partial v_i}{\partial x_j} = \frac{2v}{w} g_i n_j, \quad \frac{\partial^2 v_i}{\partial x_j \partial x_k} = \frac{4v}{w^2} g_i n_j n_k, \quad (i, j, k = 1, 2) \tag{60}$$

This deformation field is no longer as simple as the virtual deformation field of the statically admissible state. The following strain rates and strain gradient rates (all are plastic rates during collapse and hence we omit their superscript 'p') can then be obtained from Eq. (60):

$$\begin{cases} \dot{\varepsilon}_{11} = 2vg_1n_1/w \\ \dot{\varepsilon}_{22} = 2vg_2n_2/w \\ \dot{\varepsilon}_{12} = \dot{\varepsilon}_{21} = v(g_1n_2 + g_2n_1)/w \\ \dot{\eta}_{111} = 4vg_1n_1^2/w^2 \\ \dot{\eta}_{112} = 4vg_2n_1^2/w^2 \\ \dot{\eta}_{121} = \dot{\eta}_{211} = 4vg_1n_1n_2/w^2 \\ \dot{\eta}_{122} = \dot{\eta}_{212} = 4vg_2n_1n_2/w^2 \\ \dot{\eta}_{221} = 4vg_1n_2^2/w^2 \\ \dot{\eta}_{222} = 4vg_2n_2^2/w^2 \end{cases} \tag{61}$$

In conjunction with Eqs. (33) and (61), the rate of plastic dissipation (per unit volume) in the parallelogram $ABCD$ is obtained as:

$$\hat{\Phi} = \frac{2kv\sqrt{(1 + \sin^2\phi) + 8l^2/w^2}}{w\sqrt{6\alpha^2 + 1}} \tag{62}$$

For this plane strain problem, we consider a unit thickness for the sample. The (horizontal) width of the sample may also be assumed to be unity, so that the length of the slip line AB is equal to $1/\cos\beta$. Thus the volume of the parallelogram $ABCD$ is $w/(2\cos\beta)$. In view of (62), the total rate of internal energy dissipated along the slip line AB in the upper half of the sample is given by:

$$\hat{D} = \hat{\Phi}\frac{w}{2\cos\beta} = \frac{kv\sqrt{(1 + \sin^2\phi) + 8l^2/w^2}}{\cos\beta\sqrt{6\alpha^2 + 1}} \tag{63}$$

The rate of work of the external forces on the same portion of the sample is:

$$\dot{W} = T^0 v\cos(\phi - \beta) \tag{64}$$

To find an upper bound, we set the external work rate in (64) equal to the dissipation rate in (63) to give:

$$T^0 = \frac{k\sqrt{(1 + \sin^2\phi) + 8l^2/w^2}}{\cos\beta\cos(\phi - \beta)\sqrt{6\alpha^2 + 1}} \tag{65}$$

This equation indicates that, in the presence of gradient effects, the velocity still serves as a virtual quantity (as with conventional limit analysis).

Eq. (65) gives a general upper bound for T^0. The smallest one corresponds to the best upper bound on T^0 which we are seeking. This may be achieved by setting the β-derivative of the right-hand side of (65) equal to zero. This leads to:

$$\beta_m = \frac{\phi}{2} \tag{66}$$

Consequently, the upper bound for T^0 is:

$$T^0_{\mathrm{U}} \leqslant T^0 = \frac{k\sqrt{(1+\sin^2\phi)+8l^2/w^2}}{\cos^2(\phi/2)\sqrt{6\alpha^2+1}} \tag{67}$$

In conjunction with Eq. (58), the above result may be further rewritten as:

$$T^0_{\mathrm{U}} = \frac{2k\sqrt{(1+6\alpha^2)+8l^2(1-3\alpha^2/w^2)}}{(\sqrt{1-3\alpha^2}+\sqrt{1-12\alpha^2})\sqrt{6\alpha^2+1}} \tag{68}$$

When the gradient terms are neglected, so that the term $8l^2(1-3\alpha^2)/w^2$ vanishes, the conventional upper bound T^0_{UC} is recovered:

$$T^0_{\mathrm{UC}} = \frac{2k}{\sqrt{1-3\alpha^2}+\sqrt{1-12\alpha^2}} \tag{69}$$

Note that this result can also be found by setting $w/l = +\infty$ in Eq. (68). Further simplification of Eq. (68) may be made by letting $\alpha = 0$. This simplified case corresponds to an upper bound for the generalised von Mises yield criterion:

$$T^0_{\mathrm{U}} = k\sqrt{1+8l^2/w^2} \tag{70}$$

As can be seen from (68), the upper bound for the shear force T^0 depends not only on the model constants α and k, but also on the ratio of the shear band width over the internal length scale w/l. This dependence is depicted in Fig. 6. Six sets of w/l are adopted: 2, 3, 5, 7, 10 and infinity. For all cases of w/l, larger values of α

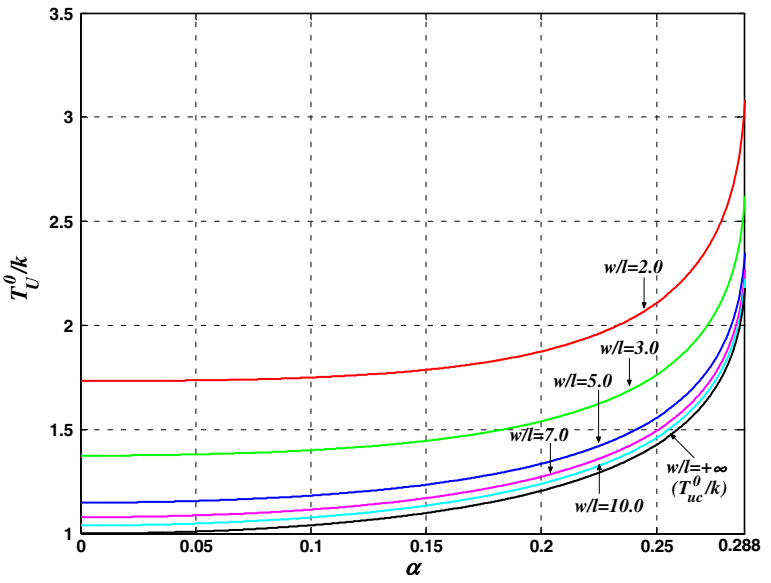

Fig. 6. The normalised upper bound T^0_{U} with relation to α and w/l.

generally correspond to larger values of T_U^0/k. The maximum value of T_U^0/k is achieved when α reaches $1/\sqrt{12}$, while the smallest value is obtained at $\alpha = 0$. For a fixed value of α, smaller values of w/l correspond to larger values of T_U^0/k. The conventional upper bound T_{UC}^0/k lies below all other curves with gradient effects. As expected, when w/l is sufficiently large ($w/l \geqslant 10$), the curve for T_U^0/k becomes very close to that of the conventional upper bound $T_{UC}^0/k(w/l = \infty)$. Thus the gradient-dependent upper bound T_U^0/k is always larger than the conventional one. This can also be deduced directly by comparing Eqs. (68) and (69). With an extra non-negative term in the numerator, the gradient-dependent upper bound will always be larger than the conventional one. In addition, it is found that, for all values of w/l and α, $T_U^0 \geqslant k$.

It is noteworthy that the introduction of strain gradients, and consequently the internal length scale l, restricts the conventional assumption that the shear band width w can be zero. Indeed Eq. (68) predicts that, if $w = 0$, the term $8l^2(1 - 3\alpha^2)/w^2$ will become infinitely large so that the upper bound of T^0 will also become unrealistically infinite. Therefore, the internal length scale l acts here as a constitutive limiter to confine the plastic deformation within a finite but non-zero width.

Regarding the band width, another interesting observation can be made. As previously noted, T_U^0 exhibits no obvious difference with T_{UC}^0 when $w/l \geqslant 10$, which implies that the gradient effects are no longer significant. Experimental observations of geomaterial behaviour frequently confirm the following four stages during the development of failure: (1) a homogeneous deformation stage; (2) a diffused deformation stage; (3) an intensely deformed shear banding stage; and (4) a macroscopic fracturing stage. From Stage (1) to Stage (4), the value of w/l can be interpreted to progressively change from very large values to very small ones. During the first two stages of deformation, w/l is sufficiently large so that gradient effects remain negligible. From the third stage onwards, when intense shear banding occurs, w/l becomes so small ($w/l \leqslant 10$ for this case) that the microstructures become comparable in size to the shear band dimension. The gradient effects are no longer negligible and influence the mechanical response markedly. Interestingly, in conventional limit theorems, the latter stages are not accounted for in the material failure model. This suggests that the corresponding compatible collapse mechanism may not necessarily be physically reasonable. The current gradient-dependent upper-bound analysis exhibits a possible interpretation for the microscopic evolution of failure, and thus has an advantage over a conventional one.

From the above it is clear that the shear band width plays a central role and, hence, should be selected with care. From both experimental observations we know that generally $w \ll h$. For a simple shear problem, Zhao et al. (2005) has developed an analytical solution for w for a gradient-dependent infinite layer under simple shear. However, the shear band treated therein was assumed to be a horizontal band governed by a gradient-enhanced damage model with a softening branch, and no dilation was considered. Nevertheless, the basic analysis approach used is still applicable here in deriving the expression of shear band width w in relation to the internal length scale l, the layer height h, and other model parameters. This will be investigated in a future paper together with other complex problems frequently observed in geotechnical applications.

3.3.3. Comparison with experimental results

The lower and upper bounds obtained above for the simple shear test will in the following be used to predict the bounds for some real soils. It has long been recognised that natural undisturbed soils have complex microstructures that make them exhibit higher strength than reconstituted soils. We assume that part of the behaviour of these microstructures in natural soils can be addressed by strain gradient theory, so that the preceding limit analysis can be used to investigate the load bounds for these soils. Four sets of experimental data on intact natural clays reported in Burland et al. (1996) are chosen here for this purpose. The strength characteristics of the four clays in terms of the frictional angle ϕ and the cohesion c^* (normalised with respect to a pressure σ_{ve}, where σ_{ve} is the equivalent pressure on the compression curve of the reconstituted soil corresponding to the void ratio of the natural soil at yield, see, Burland et al., 1996) are presented in Table 1.

We now consider a soil specimen of height h for any of the four clays and subjected to simple shear deformation. The lower and upper bounds for the ultimate shear force are sought. Before going through the calculations, however, we need to interpret the Mohr–Coulomb strength parameters in terms of the corresponding parameters used in the Drucker–Prager criterion. The friction coefficient α is given directly by Eq. (58) in terms of ϕ, whereas, under plane strain conditions, the cohesion coefficient k is given by

Table 1
Predicted lower and upper bounds of the shear force for four natural clays (data from Burland et al., 1996)

Experimental data				Other parameters					Lower bound		Upper bound	
Site of clay	ϕ	c^*	σ_{ve} (MPa)	α	k^*	$\frac{h}{l}$	$\frac{\mu_1}{\mu_2}$	$\frac{w}{l}$	$T^{0^*}_{\mathrm{LC}}$	$T^{0^*}_{\mathrm{L}}$	$T^{0^*}_{\mathrm{UC}}$	T^{0*}_{U}
Pietrafitta	24.5°	0.18	0.49	0.1344	0.1593	20.0	1.0	2.5	0.1593	0.1645	0.1715	0.2481
Todi	20.4°	0.17	2.80	0.1139	0.1562	20.0	1.0	2.5	0.1562	0.1613	0.1645	0.2407
Vallaericca	21.4°	0.26	0.90	0.1190	0.2369	20.0	1.0	2.5	0.2369	0.2447	0.2507	0.3659
Corinth maril	31.1°	0.45	0.47	0.1650	0.3639	20.0	1.0	2.5	0.3693	0.3814	0.4152	0.5887

$k^* = 3c^* \cos\phi/\sqrt{9 + 3\sin^2\phi}$. For all four clays, we assume $h/l = 20$ and a gradient-dependent stiffness identical to the conventional stiffness so that $\mu_1/\mu_2 = 1$. To define the kinematic collapse pattern, we adopt a shear band width which is 2.5 times the internal length scale so that $w/l = 2.5$. Note that these assumptions are made in the absence of better information, and that accurate determination of the values for l, μ_1/μ_2 and w/l requires further experimental work. Using these parameters, the corresponding conventional and gradient-dependent lower and upper bounds for the shear force applied to the four clay specimens are presented in Table 1. In calculating the gradient-dependent lower bounds, the bound solution in Eq. (55) has been used. Note that in Table 1, the values with a superscript '*' have been normalised by the equivalent pressure σ_{ve}. For all the four clays we have $T^{0*}_{\mathrm{LC}} < T^{0*}_{\mathrm{L}} < T^{0*}_{\mathrm{UC}} < T^{0*}_{\mathrm{U}}$, so that the gradient-dependent lower and upper bounds for T are larger than the conventional lower and upper bounds, while the gradient-dependent lower bound is below the conventional upper bound. As natural soils are frequently 'stiffer', than reconstituted ones, they often sustain higher stress and deformation levels, with microstructures contributing significantly in this process. This feature is predicted by the higher bounds from the gradient theory which considers the microstructural effects. In contrast, the use of conventional limit analysis leads to underestimated collapse loads for these stiff clays.

3.4. Uniaxial compression on a gradient-dependent layer

In this section, a gradient-dependent layer under plane strain uniaxial compression is considered. A layer of height h is subjected to a compressive pressure P^0 on both ends as depicted in Fig. 7. As in Section 3.3, we assume neither higher-order surface tractions nor body forces are present. The statically admissible state shown in Fig. 7a is first considered, together with the two kinematically admissible collapse mechanisms depicted in Figs. 7b and c. The detailed derivations for the lower bound and upper bounds for the compressive pressure P^0 follow closely those described for the simple shear case discussed in previous sections.

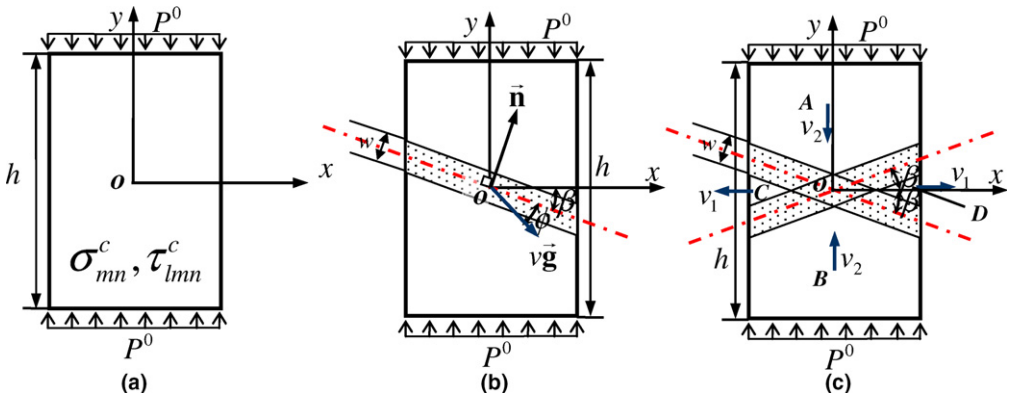

Fig. 7. Plain strain uniaxial compression of a gradient-dependent layer under: (a) statically admissible state, where σ^c_{mn} denote σ^c_{11}, σ^c_{22} and σ^c_{33}, and τ^c_{lmn} denote τ^c_{112}, τ^c_{121}, τ^c_{211}, τ^c_{222}, τ^c_{233}, τ^c_{323} and τ^c_{332}; (b) kinematically admissible state with single band; (c) kinematically admissible state with double bands.

3.4.1. A gradient-dependent lower bound for the compressive pressure P^0

For the statically admissible state depicted in Fig. 7a, it is assumed there is only one non-zero displacement in the vertical direction and that it is a function of y only: $u_2 = u_2(y) \neq 0$. Thus the non-zero strain and strain gradient components reduce to two, ε_{22} and η_{222}, which are given by: $\varepsilon_{22} = u_{2,2} = \varepsilon$ and $\eta_{222} = u_{2,22} = \varepsilon_{,2}$. For an isotropic material, the three non-zero Cauchy stresses in the sample are σ_{11}, σ_{22} and σ_{33}, while the non-zero higher-order stresses are $\tau_{112}, \tau_{121}, \tau_{211}, \tau_{222}, \tau_{233}, \tau_{323}$ and τ_{332}. Note that σ_{11}, σ_{22} and σ_{33} are all functions of ε only, and $\tau_{112}, \tau_{121}, \tau_{211}, \tau_{222}, \tau_{233}, \tau_{323}$ and τ_{332} are all functions of η_{222} only. It is further found that in this case we have $\tau_{121} = \tau_{211} = \tau_{233} = \tau_{323}$. Following the isotropic linear elastic relations defined in Appendix A, the following elastic relations are assumed:

$$\begin{cases} \sigma_{11} = \sigma_{33} = \lambda_1 \varepsilon \\ \sigma_{22} = (\lambda_1 + 2\mu_1)\varepsilon \\ \tau_{222} = l^2 \lambda_2 \varepsilon_{,2} \\ \tau_{112} = \xi_1 \tau_{222} \\ \tau_{121} = \tau_{211} = \tau_{233} = \tau_{323} = \xi_2 \tau_{222} \\ \tau_{332} = \xi_3 \tau_{222} \end{cases} \tag{71}$$

where λ_1 and μ_1 are the conventional Lame constants, λ_2 is a generalised modulus for the gradient term, and ξ_i $(i = 1, \ldots, 3)$ are non-zero coefficients representing the relative modulus between other higher-order stress components and τ_{222}. For this statically admissible state of uniaxial compression, the equilibrium equation of Eq. (16a) in the y direction has the following form:

$$\sigma_{22,2} - \tau_{222,22} = 0 \tag{72}$$

Following the same procedure as that of Section 3.3.1, σ_{22} and τ_{222} may be obtained as:

$$\frac{\sigma_{22}}{P^0} = \left(1 - \frac{1}{1 + e^{\frac{h}{l}\sqrt{\frac{\lambda_1 + 2\mu_1}{\lambda_2}}}} e^{\frac{y}{l}\sqrt{\frac{\lambda_1 + 2\mu_1}{\lambda_2}}} - \frac{1}{1 + e^{-\frac{h}{l}\sqrt{\frac{\lambda_1 + 2\mu_1}{\lambda_2}}}} e^{-\frac{y}{l}\sqrt{\frac{\lambda_1 + 2\mu_1}{\lambda_2}}} \right) \tag{73}$$

$$\frac{\tau_{222}}{lP^0} = \sqrt{\frac{\lambda^2}{\lambda_1 + 2\mu_1}} \left(\frac{1}{1 + e^{-\frac{h}{l}\sqrt{\frac{\lambda_1 + 2\mu_1}{\lambda_2}}}} e^{-\frac{y}{l}\sqrt{\frac{\lambda_1 + 2\mu_1}{\lambda_2}}} - \frac{1}{1 + e^{\frac{h}{l}\sqrt{\frac{\lambda_1 + 2\mu_1}{\lambda_2}}}} e^{\frac{y}{l}\sqrt{\frac{\lambda_1 + 2\mu_1}{\lambda_2}}} \right) \tag{74}$$

In this uniaxial compression case, the yield function of Eq. (26) reduces to:

$$f = \alpha \zeta_1 \sigma_{22} + l^{-1} \zeta_2 \tau_{222} - k = 0 \tag{75}$$

where $\zeta_1 = (3\lambda_1 + 2\mu_1)/(\lambda_1 + 2\mu_1)$ and $\zeta_2 = \sqrt{(1 + \xi_1^2 + 4\xi_2^2 + \xi_3^2)/2}$. Now consider the function $f^0 = \alpha \zeta_1 \sigma_{22} + l^{-1} \zeta_2 \, \tau_{222}$ and define the following quantity

$$A = \alpha \zeta_1 r - \zeta_2 \tag{76}$$

where $r = \sqrt{(\lambda_1 + 2\mu_1)/\lambda_2}$. If $A < 0$ then f^0 attains its maximum at $y = 0$, otherwise the maximum of f^0 is located at:

$$\frac{y_m}{h} = \frac{1}{2} \left(1 + \frac{l}{hr} \ln \left(\frac{\alpha \zeta_1 r - \zeta_2}{\alpha \zeta_1 r + \zeta_2} \right) \right) \tag{77}$$

Therefore, when $A < 0$, a lower bound for P^0 is obtained as:

$$P_{\mathrm{L}}^0 \geqslant P^0 = \left(\frac{e^{\frac{h}{l}r} + 1}{e^{\frac{h}{l}r} - 1} \right) \frac{r}{\zeta_2} k \tag{78}$$

In this case, the gradient terms dominate the lower bound. On the other hand, when f^0 is maximised at y_m in Eq. (77), the lower bound for P^0 is:

$$P^0_{\mathrm{L}} \geqslant P^0 = \frac{k}{\alpha\zeta_1 - 2\sqrt{(\alpha\zeta_1)^2 - \left(\frac{\zeta_2}{r}\right)\frac{e^{hr/2l}}{1+e^{hr/l}}}} \tag{79}$$

In this latter case, both the conventional and the gradient terms contribute to the lower bound. Following the same procedure, it is easily verified that the conventional lower bound P^0_{LC} without gradient effects is:

$$P^0_{\mathrm{LC}} \geqslant P^0 = \frac{k}{\alpha\zeta_1} \tag{80}$$

Eq. (80) can also be directly recovered from the gradient-dependent lower bound solution in Eq. (79) by letting $\zeta_2 = 0$ and $h/l = +\infty$. Since $\zeta_2 = 0$, y_m in (77) is equal to $h/2$, which means that the conventional terms dominate while the gradient terms vanish.

The lower bound (79) is compared with the conventional lower bound in Fig. 8. We assume here that $\alpha = 0.25$ and $\zeta_1 = 4$ so the conventional lower bound is $P^0_{\mathrm{LC}} = k$. We further assume $\zeta_2 = 2$, so that $r > 2$ will render $A > 0$ in (76). Six values of h/l are adopted: 2, 3, 4, 5, 6 and ∞. As may be seen, all the gradient-dependent bounds predicted by Eq. (79) are larger than the conventional ones. The bound with smaller h/l generally exhibits a higher prediction. When r becomes infinitely large, all gradient-dependent bounds coincide with the conventional one. It is also found that when $h/l \geqslant 10$, the obtained P^0_{L} will fall onto the horizontal line of the conventional bound.

3.4.2. Gradient-dependent upper bounds for P^0

Consider the two compatible collapse mechanisms illustrated in Figs. 7b and c. For the single-band case, the same procedure as for simple shear case is followed. Detailed derivations will be omitted here for briefness, and only the obtained upper bound P^0_{U} for this uniaxial compressed layer with single band is provided. It is found that when:

$$\beta_m = \frac{\pi}{4} - \frac{\phi}{2} \tag{81}$$

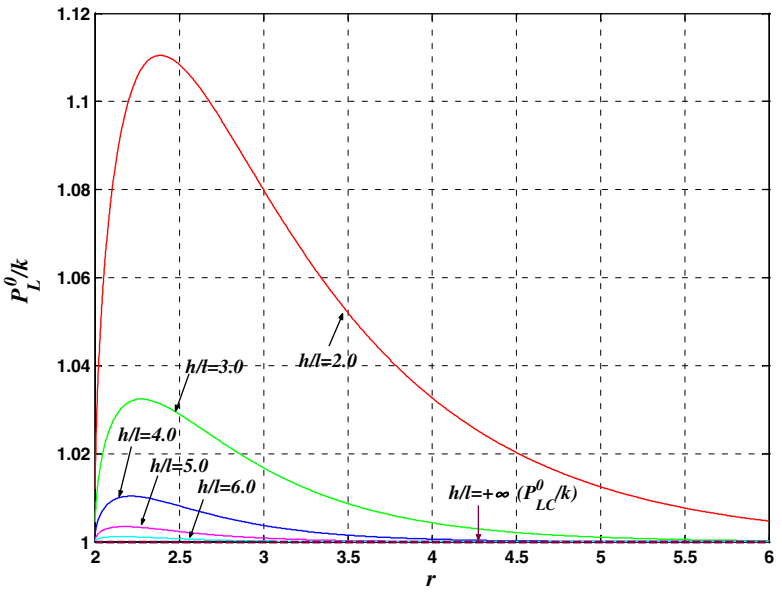

Fig. 8. Variation of P^0_{L}/k in Eq. (79) with relation to r and h/l ($\alpha = 0.25$, $\zeta_1 = 4$, $\zeta_2 = 2$).

the upper bound for P^0 is

$$P_{\mathrm{U}}^0 \leqslant T^0 = \frac{2k\sqrt{(1+\sin^2\phi)+8l^2/w^2}}{(1+\sin\phi)\sqrt{6\alpha^2+1}} \tag{82}$$

Using Eq. (58), the result in (82) may be further rewritten as:

$$P_{\mathrm{U}}^0 = \frac{2k\sqrt{(1+6\alpha^2)+8l^2(1-3\alpha^2)/w^2}}{(\sqrt{1-3\alpha^2}+3\alpha)\sqrt{6\alpha^2+1}} \tag{83}$$

Again the corresponding conventional upper bound P_{UC}^0 may be obtained by setting w/l equal to infinity to give

$$P_{\mathrm{UC}}^0 = \frac{2k}{\sqrt{1-3\alpha^2}+3\alpha} \tag{84}$$

Variation of this upper bound with respect to α and w/l, together with the conventional upper bound, will be compared with the results for the double-banded case in the following.

Consider now the double-band case as shown in Fig. 7c. Due to symmetry, we take the upper half of the sample as illustrated in Fig. 9a. It is assumed the rigid block A moves vertically at a velocity of $-v_2$ ($v_2 > 0$), while the rigid block D moves at a velocity of v_1 ($v_1 > 0$) along the x direction. It is further assumed that in the pentagon *oabcd*, the boundary *cd* has a velocity of v_2 while the boundary *ab* moves at v_1. Within this pentagon, the overall velocity field changes gradually from *cd* to *ab* over a total width of w. To facilitate an easy understanding of the velocity variation, detailed velocity distributions along all the boundaries of *oabcd* and along *ad* are depicted in Figs. 9b and c, respectively. In view of Fig. 9a, the unit normal and tangential vectors of the pentagon *oabcd* are respectively:

$$\vec{\mathbf{n}} = (n_1, n_2) = (\sin\beta, -\cos\beta), \quad \vec{\mathbf{t}} = (t_1, t_2) = (\cos\beta, \sin\beta) \tag{85}$$

To build a relation between v_1 and v_2, two points p_1 and p_2 located on neighbouring boundaries of the band are considered. The following dilatancy condition is invoked for the velocity differences between the two points:

$$[\vec{\mathbf{v}}_1 - \vec{\mathbf{v}}_2]_n = \tan\phi[\vec{\mathbf{v}}_1 - \vec{\mathbf{v}}_2]_t \tag{86}$$

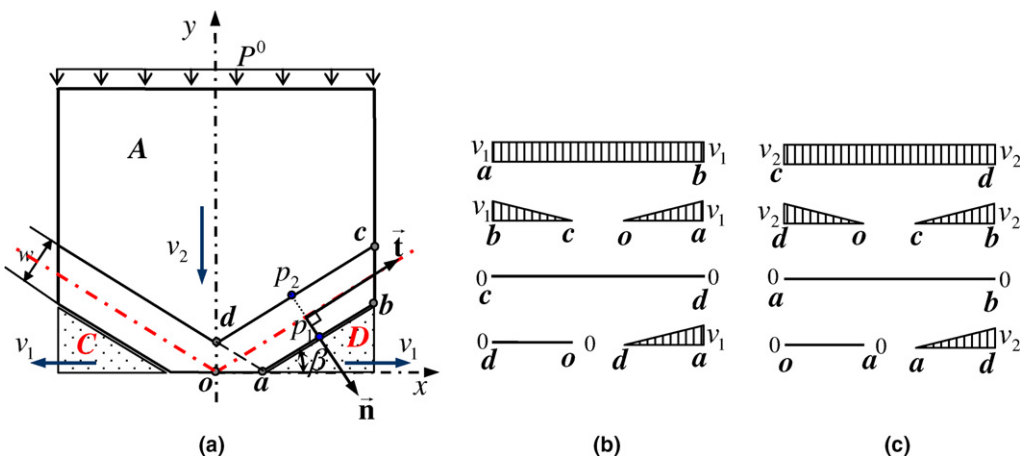

Fig. 9. Zoomed upper half configuration of Fig. 7c: (a) zoomed view; (b) horizontal velocity distribution of each boundary of the pentagon *oabcd*; (c) vertical velocity distribution of each boundary of *oabcd*.

where ϕ is the frictional angle as defined in Eq. (58). $[\vec{\mathbf{v}}_1 - \vec{\mathbf{v}}_2]_n$ and $[\vec{\mathbf{v}}_1 - \vec{\mathbf{v}}_2]_t$ are, respectively, the velocity difference of the two points in the normal direction and the tangential directions. Combining (85) and (86), we have:

$$v_1 \sin\beta - v_2 \cos\beta = \tan\phi(v_1 \cos\beta + v_2 \sin\beta) \tag{87}$$

From Eq. (87), the following relation between v_1 and v_2 is obtained:

$$v_1 = \vartheta v_2 \tag{88}$$

where $\vartheta = 1/\tan(\beta - \phi)$. In recognition of the velocity distributions within the pentagon *oabcd*, the following relations for the strain rates and strain gradient rates are obtained:

$$\begin{cases} \dot{\varepsilon}_{11} = v_1 \sin\beta / w \\ \dot{\varepsilon}_{22} = -v_2 \cos\beta / w \\ \dot{\varepsilon}_{12} = \dot{\varepsilon}_{21} = (v_2 \sin\beta - v_1 \cos\beta)/(2w) \\ \dot{\eta}_{111} = v_1 \sin^2\beta / w^2 \\ \dot{\eta}_{112} = -v_2 \sin^2\beta / w^2 \\ \dot{\eta}_{121} = \dot{\eta}_{211} = v_1 \sin\beta\cos\beta / w^2 \\ \dot{\eta}_{122} = \dot{\eta}_{212} = -v_2 \sin\beta\cos\beta / w^2 \\ \dot{\eta}_{221} = v_1 \cos^2\beta / w^2 \\ \dot{\eta}_{222} = -v_2 \cos^2\beta / w^2 \end{cases} \tag{89}$$

Using Eq. (88) to substitute for v_1 with v_2, and following the same procedure outlined in Section 3.3.2, the rate of dissipation per unit volume in the bands is obtained as:

$$\hat{\Phi} = \frac{k v_2 \sqrt{(1 + \sin^2\phi) + 2l^2/w^2}}{|\sin(\beta - \phi)| w \sqrt{6\alpha^2 + 1}} \tag{90}$$

To obtain the overall rate of internal energy dissipation, we further assume the shear band width is very small compared to the sample width. This will avoid the explicit introduction of the sample width when calculating the shear band volume. A layer of unit thickness and unit width is further assumed. The total volume of bands in the upper half of the sample can be approximated by $w/(\cos\beta)$[1], and the total rate of internal energy dissipation may be obtained as:

$$\hat{D} = \hat{\Phi}\frac{w}{\cos\beta} = \frac{k v_2 \sqrt{(1 + \sin^2\phi) + 2l^2/w^2}}{\cos\beta |\sin(\beta - \phi)| \sqrt{6\alpha^2 + 1}} \tag{91}$$

In this case, the rate of work done by the external forces on the upper half of the sample is:

$$\dot{W} = P^0 v_2 \tag{92}$$

Equating Eqs. (91) and (92) leads to the following upper bound for P^0:

$$P^0 = \frac{k \sqrt{(1 + \sin^2\phi) + 2l^2/w^2}}{\cos\beta |\sin(\beta - \phi)| \sqrt{6\alpha^2 + 1}} \tag{93}$$

The extreme value of (93) occurs at

$$\beta_m = \frac{\pi}{4} + \frac{\phi}{2} \tag{94}$$

[1] The exact volume of the band for the upper half should be $w(2W\sin\beta - w)/(2\sin 2\beta)$, where W denotes the sample width. When $W \gg w$, this volume may be approximated by $wW/\cos\beta$. Assuming $W = 1$ we have a volume of $w/\cos\beta$.

which coincides with the value predicted by Hill (1952, 2001) for a double-band formation, even in the presence of gradient terms. At β_m, the upper bound of P^0 for this double-band collapse mechanism is:

$$P^0_{\mathrm{U}'} = \frac{2k\sqrt{(1+\sin^2\phi)+2l^2/w^2}}{(1+\sin\phi)\sqrt{6\alpha^2+1}} = \frac{2k\sqrt{(1+6\alpha^2)+2l^2(1-3\alpha^2)/w^2}}{(\sqrt{1-3\alpha^2}+3\alpha)\sqrt{6\alpha^2+1}} \tag{95}$$

If $w/l=\infty$ (so that gradient terms may be neglected), a conventional upper bound with the double-band collapse mechanism is readily obtained from (95):

$$P^0_{\mathrm{U}'\mathrm{C}} = \frac{2k}{\sqrt{1-3\alpha^2}+3\alpha} \tag{96}$$

This is identical with Eq. (84) for a single band mechanism. Hence, for the two collapse patterns, the conventional upper bounds are the same: $P^0_{\mathrm{UC}} = P^0_{\mathrm{U}'\mathrm{C}}$.

Comparing the double-band upper bound obtained above with the single-band one presented in Eq. (83), one immediately finds that the bounds for the two mechanisms differ only in the coefficients of the gradient terms. If gradient effects are appreciable, the double-band upper bound is smaller than the single-band one. To illustrate their relationship more clearly, the distributions of the two bounds are plotted against α and w/l in Fig. 10. In this figure, the double-band results are denoted by solid lines, with dashed lines showing the single-band predictions. For both collapse mechanisms, the gradient dependent compressive layer attains a maximum upper bound at $\alpha=0$ for all cases of w/l, while a minimum value is obtained at $\alpha=1/\sqrt{12}$. Smaller values of w/l generally result in larger values of P^0_{U} and $P^0_{\mathrm{U}'}$. The conventional prediction ($w/l=+\infty$) is below all the other predicted curves with finite w/l. It can thus be concluded that the gradient-dependent upper bound for either the single-band or double-band mechanism is larger than its conventional counterpart. At the same values of α and w/l, the double-band mechanism leads to a smaller upper bound than the single-band one, which confirms the assertion in the beginning of this paragraph. We now have a second look at the two bounds in Eqs. (83) and (95). The coefficients of the gradient terms have led to the difference between the two bounds. We now incorporate the coefficient into the shear band width in both expressions, and assume the band width for the double-band case is half that of the single-band mechanism (the width of the sample is the same for the two cases). Given that α and l are material properties and are constant under any conditions,

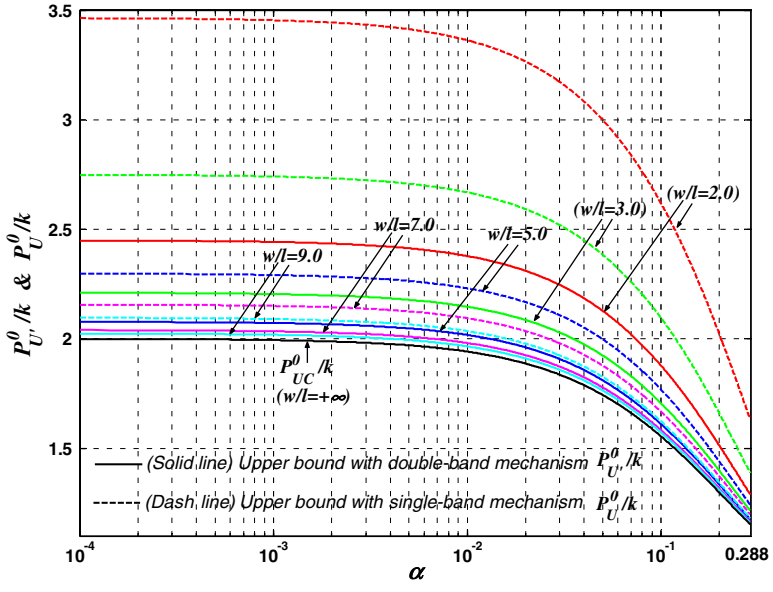

Fig. 10. Variation of normalised upper bounds P^0_{U} for single-band (dashed lines) and $P^0_{\mathrm{U}'}$ for double-band (solid lines) collapse mechanism with relation to α and w/l.

we readily find that the two expressions predict the same upper bound for the uniaxial compression test. In other words, at the same collapse load, a wider band width for the single-band failure is expected, while for a double-band mechanism, thinner failure zones with roughly half width of that of the single-band mechanism will be found. It is easy to interpret this from an energy point of view. For a sample at a certain collapse load level, the mechanical energy dissipated in driving the development of microstructural deformation and macroscopic shear bands is fixed, and so is the effective volume of the shear bands. Hence, if the band length for the double-band case is double that of the single-band one, the band width for the former will certainly be smaller than the latter. The inclusion of gradient terms again takes into account the effect of microstructures on the upper bounds for different collapse mechanisms, which is an improvement on the conventional theory.

3.4.3. Comparison with experimental results

The above lower and upper bounds for uniaxial compression tests are now compared with experimental data. As uniaxial compression tests (UC) are rarely conducted for soils, due to the loose properties of these materials, we have chosen a set of data for rocks for the comparison. The results are from the experiments conducted by Papamichos et al. (2000) for Red Wildmoor (RW) sandstone. Over 10 specimens were tested under uniaxial compression conditions and many others underwent conventional triaxial compression and plane biaxial compression. The strength parameters of RW sandstone, however, were derived only from triaxial and biaxial tests and given in terms of the frictional angle ϕ and cohesion c. The obtained strength parameters were $\phi = 42.6°$ and $c = 2.73$ MPa for samples under humid conditions (Table IX therein). Even though the corresponding strength indices may vary for uniaxial compression conditions, we still use the above parameters for a preliminary investigation of the load capacity on RW sandstone sample under uniaxial compression conditions.

Using Eq. (58) and the relation $k = 3c\cos\phi/\sqrt{9 + 3\sin^2\phi}$, the equivalent strength parameters for the plane strain Drucker–Prager criterion are $\alpha = 0.2101$ and $k = 1.8717$ MPa. The experiments also provided useful information on the average grain size D_{50} and shear band width w as follows: $D_{50} = 0.107$ mm, $w = 4.5D_{50}$. We further assume that the internal length scale l is 3 times D_{50}: $l = 3D_{50}$. For the uniaxial compression case, we assume only the axial higher stress dominates so that $\xi_1 = \xi_2 = \xi_3 = 0$ in Eq. (71). This leads to $\zeta_2 = 0.71$. We further assume the gradient modulus is comparable to the conventional one, so that $\lambda_1 = \lambda_2$. Using average elastic parameters for specimens in the uniaxial compression tests ($E = 1938$ MPa, $v = 0.38$, excluding those with $v > 0.5$ and those not failed) and assuming plane strain conditions, we adopted a value of $\zeta_1 = 4.17$. For the lower bound analysis, it is readily verified that the combination of the above parameters leads to $A > 0$, so that Eqs. (79) and (80) can be used, respectively, to compute the gradient-dependent and conventional lower bounds. As the specimens used in the experiments were either 50.8 mm or 101.6 mm in height, the ratio h/l for this case is so large that the gradient effects in the lower bound expression become negligible. Hence the gradient-dependent lower bound computed from Eq. (79) is approximately the same as the conventional one obtained from Eq. (80): $P^0_{\mathrm{L}} \doteq P^0_{\mathrm{LC}} = 2.138$ MPa. The gradient-dependent and conventional upper bounds can be obtained by using Eqs. (83), (84) and (95) as: $P^0_{\mathrm{UC}} = 2.3968$ MPa, $P^0_{\mathrm{U}} = 4.445$ MPa, $P^0_{\mathrm{U}'} = 3.041$ MPa. Immediately, we see that $P^0_{\mathrm{LC}} = P^0_{\mathrm{L}} < P^0_{\mathrm{UC}} < P^0_{\mathrm{U}'}, < P^0_{\mathrm{U}}$, which appears reasonable for the load capacity of the uniaxial compression problem.

When these predicted bounds for P^0 are further compared with experimental results of uniaxial compression tests in Papamichos et al. (2000), it is found that the smallest peak axial compressive stress obtained in the experiments (4.5 MPa for the specimen CAV9508) is larger than P^0_{U}. Several possible reasons may give rise to the above discrepancy. Firstly, the experimental strength parameters for RW sandstone were derived from conventional triaxial and biaxial compression tests, whereas the problem considered is a plane strain uniaxial compression case. As remarked by Bishop (1966), the friction angle in the plane strain case is generally larger than in the triaxial case. The cohesion may also vary for the two cases. In addition, the assumed parameters for the bound calculation (l, ζ_2 and λ_2) may deviate markedly from their real values. Thus, using appropriate strength indices and model parameters for the bound computation may reduce the above discrepancy. Secondly, the actual stress field in the uniaxial compression tests is truly three-dimensional, and the plastic deformation may involve complex hardening and softening behaviour. Moreover, it is further complicated by the possible existence of random heterogeneous imperfections in the testing specimens. Our plane strain assump-

tion for the problem, and the simplification inherent in an elastic perfectly-plastic constitutive relation for a homogenous material, will also contribute error in the limit load prediction. Thirdly, uniaxially compressed specimens may undergo severe fragmentation, as remarked by Vardoulakis et al. (1998). This can lead to complicated mechanical behaviour accompanying the emergence of micro- and macro-cracks in the specimen, and frequently lead to axial splitting failures. The limit formulations derived here are inappropriate for modelling this mode of failure.

4. Conclusions

The limit theorems proposed by Drucker et al. (1952) and Drucker and Prager (1952) are reformulated within the framework of strain gradient plasticity. Equilibrium equations and boundary conditions with consideration of gradient terms are developed, and the lower and upper theorems are rephrased for gradient-dependent materials. A generalised Drucker–Prager yield criterion is proposed to consider geomaterials with hydrostatic stress dependence and gradient effects. Analytical solutions for two generalised plane strain problems are found and compared with those obtained from conventional theories. The influence of gradient effects on these solutions is addressed.

Through two plane strain examples, it is shown that the inclusion of gradient terms makes the lower-bound solutions dependent on the conventional to higher-order elastic modulus ratio, the sample size to internal length scale ratio, as well as the strength parameters. For the upper bounds, the influence of the gradient terms is primarily controlled by the ratio of the shear band-width to the internal length scale. It is shown that this length scale is a constitutive limiter and prevents the localised shear band width from being zero. The internal length scale also allows us to address the influence of size effects on the strength of geomaterials. It is illustrated that collapse loads are generally higher for smaller samples and/or narrower shear band formations, and vice versa. Qualitative comparisons of the bound results with experimental data have also been given.

Using the principles and procedures outlined in this paper, other applications like simple bending and axi-symmetric loading problems with gradient effects are also treatable. This will be a topic of future work.

Acknowledgements

The first author is grateful to Dr. Andrei Lyamin for his careful proofreading of the manuscript. The authors also thank the two anonymous reviewers for their helpful comments on improving the quality of this paper.

Appendix A. Isotropic linear elastic strain gradient theory of Mindlin (1965)

In this paper, the following generalised Hooke's theory of Mindlin's (1965) is used to describe the strains and strain gradients in linear elastic isotropic material, with the second-order gradient of strains being neglected (see Eq. (20) therein):

$$\sigma_{ij} = \lambda_1 \varepsilon_{kk} \delta_{ij} + 2\mu_1 \varepsilon_{ij} \tag{A.1}$$

$$\tau_{ijk} = a_1(\eta_{ipp}\delta_{jk} + \eta_{jpp}\delta_{ik}) + \frac{1}{2}a_2(\eta_{ppi}\delta_{jk} + 2\eta_{kpp}\delta_{ij} + \eta_{ppj}\delta_{ik}) + 2a_3\eta_{ppk}\delta_{ij} + 2a_4\eta_{ijk} + a_5(\eta_{kji} + \eta_{kij}) \tag{A.2}$$

Appendix B. Proof of the gradient-dependent lower-bound theorem in Section 2.4.1

The proof of the gradient-dependent lower-bound theorem is similar to that for the conventional lower-bound theorem given by Chen and Han (1988). To prove this theorem, we show that assuming it to be false results in a contradiction. If the body under the loads T_k, R_k and F_k collapses, the failure mode is associated with the actual stresses, higher order stresses, strain rates, strain gradient rates, and displacement rates

σ^{c}_{ij}, τ^{c}_{ijk}, $\dot{\varepsilon}^{c}_{ij}$, $\dot{\eta}^{c}_{ijk}$ and v^{c}_{i}. This collapse pattern corresponds to the collapse loads T_k on S_T, R_k on S_R and F_k in V, with $v^{c}_{i}=0$ and $n_l\partial_l v_i=0$ on S_u. There may be two equilibrium systems existing: T_k, R_k, F_k, σ^{c}_{ij}, τ^{c}_{ijk} and T_k, R_k, F_k, σ^{E}_{ij}, τ^{E}_{ijk}. From the virtual work equation in (15), we have:

$$\int_s (T^{c}_{i}v^{c}_{i}+R^{c}_{i}n_k\partial_k v^{c}_{i})\,\mathrm{d}S+\int_V F^{c}_{i}v^{c}_{i}\,\mathrm{d}V=\int(\sigma^{c}_{ij}\dot{\varepsilon}^{c}_{ij}+\tau^{c}_{ijk}\dot{\eta}^{c}_{ijk})\,\mathrm{d}V \tag{B.1}$$

$$\int_s (T^{c}_{i}v^{c}_{i}+R^{c}_{i}n_k\partial_k v^{c}_{i})\,\mathrm{d}S+\int_V F^{c}_{i}v^{c}_{i}\,\mathrm{d}V=\int(\sigma^{E}_{ij}\dot{\varepsilon}^{c}_{ij}+\tau^{E}_{ijk}\dot{\eta}^{c}_{ijk})\,\mathrm{d}V \tag{B.2}$$

Hence,

$$\int_v((\sigma^{c}_{ij}-\sigma^{E}_{ij})\dot{\varepsilon}^{c}_{ij}+(\tau^{c}_{ijk}-\tau^{E}_{ijk})\dot{\eta}^{c}_{ijk})\,\mathrm{d}V=0 \tag{B.3}$$

Since we assume that all deformation at collapse is plastic, (B.3) becomes

$$\int_v((\sigma^{c}_{ij}-\sigma^{E}_{ij})\dot{\varepsilon}^{pc}_{ij}+(\tau^{c}_{ijk}-\tau^{E}_{ijk})\dot{\eta}^{pc}_{ijk})\,\mathrm{d}V=0 \tag{B.4}$$

In the compound space of stresses and higher order stresses, the properties of convexity and normality to the yield surface require that:

$$(\sigma^{c}_{ij}-\sigma^{E}_{ij})\dot{\varepsilon}^{pc}_{ij}+(\tau^{c}_{ijk}-\tau^{E}_{ijk})\dot{\eta}^{pc}_{ijk}>0 \tag{B.5}$$

for any σ^{E}_{ij} and τ^{E}_{ijk} below yield. Therefore, the sum of positive terms cannot vanish and Eq. (B.4) cannot be true. The gradient-dependent lower-bound theorem is thus proved. If $f(\sigma^{E}_{ij},\tau^{E}_{ijk})=0$ is permitted, then the material body may be at the point of collapse.

Appendix C. Proof of the gradient-dependent upper-bound theorem in Section 2.4.2

We prove the gradient-dependent upper-bound theorem using an apagogical approach, which is similar to the proof for the conventional upper-bound theorem given by Chen and Han (1988). We show that assuming the theorem to be false leads to a contradiction.

For a kinematically compatible mechanism with plastic deformation $\dot{\varepsilon}^{k}_{ij}$ and $\dot{\eta}^{k}_{ijm}$, v^{k}_{i} and Dv^{k}_{i} which satisfies the conditions $v^{k}_{i}\equiv 0$ and $Dv^{k}_{i}\equiv 0$ on the displacement boundary S_u, the loads determined by choosing the equality case of inequality (19) are assumed to be T_k, R_k and F_k. Now assume that these loads are less than the actual limit loads, so that the material body will not collapse at this level of loading. An equilibrium distribution of stresses σ^{E}_{ij} and higher order stresses τ^{E}_{ijk} therefore exists which everywhere in the body are below yield $f(\sigma^{E}_{ij},\tau^{E}_{ijk})<0$. From the principle of virtual work of Eq. (15), we have:

$$\int_S (T_i v^{k}_{i}+R_i Dv^{k}_{i})\,\mathrm{d}S+\int_V F_i v^{k}_{i}\,\mathrm{d}V=\int(\sigma^{E}_{ij}\dot{\varepsilon}^{k}_{ij}+\tau^{E}_{ijk}\dot{\eta}^{k}_{ijk})\,\mathrm{d}V \tag{C.1}$$

Since we obtained T_k, R_k and F_k by equating the two sides of inequality (19), in view of Eq. (20) and (C.1), we have:

$$\int_v[(\sigma^{k}_{ij}-\sigma^{E}_{ij})\dot{\varepsilon}^{k}_{ij}+(\tau^{k}_{ijk}-\tau^{E}_{ijk})\dot{\eta}^{k}_{ijk}]\,\mathrm{d}V=0 \tag{C.2}$$

As σ^{E}_{ij} and τ^{E}_{ijk} are below yield while σ^{k}_{ij} and τ^{k}_{ijk} are on the yield surface, the properties of convexity and normality require

$$(\sigma^{k}_{ij}-\sigma^{E}_{ij})\dot{\varepsilon}^{k}_{ij}>0,\quad\text{and}\quad(\tau^{k}_{ijk}-\tau^{E}_{ijk})\dot{\eta}^{k}_{ijk}>0 \tag{C.3}$$

(C.2) and (C.3) are in obvious contradiction to each other. The gradient-dependent upper-bound theorem is thus proved.

References

Bishop, A.W., 1966. The strength of soils as engineering materials. Six Rankine lecture. Géotechnique 16 (2), 91–130.
Burland, J.B., Rampello, S., Georgiannou, V.N., Calabresi, G., 1996. A laboratory study of the strength of four stiff clays. Géotechnique 46 (3), 491–514.
Chambon, R., Caillerie, D., Tamagnini, C., 2004. A strain space gradient plasticity theory for finite strain. Comput. Methods Appl. Mech. Eng. 193, 2797–2826.
Chen, W.F., Han, D.J., 1988. Plasticity for Structural Engineering. Springer, New York.
Collins, I.F., 2005. Elastic/plastic models for soils and sands. Int. J. Mech. Sci. 47, 493–508.
Drucker, D.C., Prager, W., 1952. Soil mechanics and plastic analysis for limit design. Quart. Appl. Math. 10, 157–165.
Drucker, D.C., Prager, W., Greenberg, H.J., 1952. Extended limit design theorems for continuous media. Quart. Appl. Math. 9, 381–389.
Fleck, N.A., Hutchinson, J.W., 1993. A phenomenological theory for strain gradient effects in plasticity. J. Mech. Phys. Solids 41 (12), 1825–1857.
Fleck, N.A., Hutchinson, J.W., 1997. Strain gradient plasticity. In: Hutchinson, J.W., Wu, T.Y. (Eds.), Advances in Applied Mechanics, vol. 33. Academic Press, New York, pp. 295–361.
Germain, P., 1973. The method of virtual power in continuum mechanics. Part 2: Microstructure. SIAM. J. Appl. Math. 25 (3), 556–575.
Hill, R., 1952. On discontinuous plastic states, with special reference to localized necking in thin sheets. J. Mech. Phys. Solids 1, 19–30.
Hill, R., 2001. On the mechanics of localized necking in anisotropic sheet metals. J. Mech. Phys. Solids 49, 2055–2070.
Mindlin, R.D., 1964. Micro-structure in linear elasticity. Arch. Ration. Mech. Anal. 16, 51–78.
Mindlin, R.D., 1965. Second gradient of strain and surface tension in linear elasticity. Int. J. Solids Struct. 28, 845–857.
Papamichos, E., Tronvoll, J., Vardoulakis, I., Labuz, J.F., Skjaerstein, A., Unander, T.E., Sulem, J., 2000. Constitutive testing of Red Wildmoor sandstone. Mech. Cohesive Mater. 5, 1–40.
Smyshlyzev, V.P., Fleck, N.A., 1996. The role of strain gradients in the grain size effect for polycrystals. J. Mech. Phys. Solids 44 (4), 465–495.
Toupin, R.A., 1962. Elastic materials with couple stresses. Arch. Ration. Mech. Anal. 11, 385–414.
Vardoulakis, I., Graf, B., 1985. Calibration of constitutive models for granular materials using data from biaxial experiments. Géotechnique 35, 299–317.
Vardoulakis, J., Labuz, J.F., Papamichos, E., Tronvoll, J., 1998. Continuum fracture mechanics of uniaxial compression on brittle materials. Int. J. Solids Struct. 35 (31–32), 4313–4335.
Zhao, J.D., Sheng, D.C., Zhou, W.Y., 2005. Shear banding analysis of geomaterials by strain gradient enhanced damage model. Int. J. Solids Struct. 42 (20), 5335–5355.
Zhao, J.D., Sheng, D.C, 2005. Strain gradient plasticity by internal-variable approach with normality structure. Int. J. Solids Struct. (in press), doi:10.1016/j.ijsolstr.2005.09.006.